Journal of Building Engineering 108 (2025) 112819

Contents lists available at ScienceDirect

Journal of Building Engineering

journal homepage: www.elsevier.com/locate/jobe

Comprehensive study of GFRP bar-concrete bond behavior using pull-out and three-point bending tests

Mohammod Minhajur Rahman [a], Charles T. Cope III [a], Iman Abavisani [a], Tommaso D'Antino [b,*], Francesco Focacci [c], Christian Carloni [a]

[a] Department of Civil and Environmental Engineering, Case Western Reserve University, Cleveland, OH, USA
[b] Department of Architecture, Built Environment, and Construction Engineering (ABC), Politecnico di Milano, Milan, Italy
[c] eCampus University, Novedrate, Italy

ARTICLE INFO

Keywords:
GFRP bars
Bond
DIC
Pull-out
Bending test

ABSTRACT

The GFRP bar-concrete bond behavior is known to be influenced by factors such as bar surface treatment, bar diameter, and concrete strength. This study aims to provide a comprehensive understanding of the bond behavior of GFRP bars embedded in concrete. Pull-out specimens are cast from two concrete batches with different compressive strengths. Two surface coating conditions are considered, i.e., one with a lacquer finish and one without. Specimens with three bonded lengths are used to determine the role of the bonded length in the bond mechanism (i.e., $5d_b$, $10d_b$, and $20d_b$, where d_b = nominal bar diameter). Two free end conditions of the pull-out specimens are examined: one with the bar protruding at the free end and another with the bar cut at the free end (i.e., the bar is cut flush with the concrete surface). The pull-out test responses are analyzed in terms of applied load versus loaded end slip and free end slip. Three-point bending (TPB) tests are conducted on concrete notched beams with two different widths (75 mm and 150 mm). Beams are either reinforced with a single GFRP bar or they are not reinforced and used as benchmark. Notched beams are only cast from one of the concrete batches used for the pull-out test specimens. This study shows how the protrusion of the bar can affect the bond strength in pull-out tests. In addition, the different bond behavior of the GFRP bars observed in pull-out tests and TPB tests of notched beams is discussed considering the length of the stress transfer zone for bars with different surface conditions.

1. Introduction

Glass fiber-reinforced polymer (GFRP) bars offer inherent benefits including low density, high strength, resistance to corrosion, and non-magnetic nature [1–8]. These advantages over steel bars have led to extensive use of GFRP bars in marine environments and in bridge decks, where chloride attacks are common and typically result in the degradation of steel reinforcing bars [9–14]. Despite these benefits, GFRP bars still pose some drawbacks such as linear elastic behavior almost up to peak load or lack of ductility, difficulties in bending the bars, poor resistance to high temperatures [15–17], and poor shear strength. In addition, GFRP bars have an elastic modulus equal to 20–25 % that of steel bars and their bond with concrete is affected by different bar surface treatments (e.g., sand coating, spiral winding, grooving, resin ribs) [18–24], bar diameter d_b [25], concrete strength [26], concrete cover [27], and bar

* Corresponding author.
E-mail address: tommaso.dantino@polimi.it (T. D'Antino).

https://doi.org/10.1016/j.jobe.2025.112819
Received 19 August 2024; Received in revised form 15 April 2025; Accepted 30 April 2025
Available online 2 May 2025

position [28–31].

Crack initiation and propagation in a concrete structure reinforced with GFRP bars depend on the stress transfer between the reinforcement and concrete and on the mechanical properties of concrete and bar [28]. Understanding the behavior of the bar-concrete bond is crucial. Over the past decade, extensive research has focused into the behavior of the bond between GFRP bar and concrete, and various factors outlined earlier have been investigated. Pull-out tests are commonly used to experimentally investigate bar-bond behavior due to their simple setup and direct application of the pull-out force. The required bonded length (ℓ) for the pull-out test, as per ASTM D7913 [32] and ISO 10406-1 [33], is $5d_b$ and $4d_b$ (d_b = bar diameter), respectively. Recently, the authors have investigated the effect of GFRP bar diameter [34] and free end protruding portion of the GFRP bar [35] on GFRP bar-concrete bond behavior using pull-out tests. It was found that the axial stress at peak load using smaller diameter bars was higher compared to the larger diameter bars [34]. This trend depends on the stress-transfer mechanism between the bar and concrete and different behaviors were observed in the literature [36,37]. In the other study, the protruding portion of the GFRP bar was found to provide higher peak loads compared to specimens without any protrusion [35]. For $5d_b$ and $20d_b$ bonded length specimens, the increase in peak loads was 142 % and 28 %, respectively. Furthermore, the authors have also calibrated an interfacial cohesive material law (CML) using pull-out test results from a previous study [28], with different bonded length specimens [38] and with different free end conditions in pull-out specimens [35].

A study of the influence of elevated temperatures on the bond properties of GFRP bar-concrete was conducted through pull-out tests with a bonded length of $5d_b$ in Ref. [39]. The test results indicated a 34 % reduction in bond strength (i.e., average interfacial shear stress at peak load) for ribbed GFRP bars (glass transition temperature $T_g = 104\ ^\circ C$) at 100 °C compared to ambient temperature, while sand-coated bars (glass transition temperature $T_g = 98\ ^\circ C$) exhibited an 80 % reduction. These results highlight the combined effect of environmental conditions and the surface characteristics of the GFRP bar. The effect of the bonded length was examined for a sand-coated GFRP bar by the authors [28]. Additionally, the same study showed no discernible impact of concrete age; the concrete strength ranged between 34 MPa and 46 MPa. For bonded lengths greater than $10d_b$, ACI 440.1R-15 predicted a greater bonded length necessary to achieve a specific stress in the bar compared to values obtained from pull-out tests presented in the study. The effect of bonded length was also investigated by Ref. [40] using carbon FRP bars where they found that the bond strength decreased as the bonded length increased. The effect of bonded length was also investigated in Refs. [41,42]. The effect of surface condition and bar location was investigated by another study [29] using a hinged beam. Two surface conditions were explored: one with helical wrapping and fine sand coating (max sand diameter equal to 0.5 mm), and the other with only fine sand coating (max diameter equal to 0.5 mm). The study indicated a higher bond strength for the latter condition. Moreover, when the bar was positioned at the top of the beam, the bond strength was found to be lower compared to its placement at the bottom. In a related study [26], variations in bond strength and failure modes corresponding to changes in concrete compressive strength were reported. Namely, failure occurred within the bar or within concrete for high- and low-strength concrete, respectively. Interestingly, the research concluded that the impact of bar surface treatment on bond strength was less significant in low-strength concrete when compared to high-strength concrete. In a recent study by the authors [43], the GFRP bar-concrete bond behavior was investigated by performing three-point bending (TPB) tests on concrete notched beams reinforced with a GFRP bar. In that study, the GFRP bar force and slip from the notched beam tests were compared with responses from the pull-out tests of the same bonded length. It was found that the responses initially matched. Afterwards, a higher rate of load increment was observed for the pull-out test responses, indicating that the pull-out responses were an upper bound. However, the study did not conduct a comprehensive pull-out test campaign using the same concrete to examine the other influencing factors for GFRP bar-concrete bond behavior discussed earlier.

A comprehensive test campaign of pull-out tests is essential for understanding the GFRP bar-concrete bond behavior. Additionally, testing a small-scale notched beam reinforced with a GFRP bar in a TPB setup can serve as an intermediate test between pull-out tests and full-scale beam tests to study the bond behavior in the presence of a bending moment. In this paper, pull-out tests are conducted to investigate the influence of concrete strength, surface condition, and bonded length. Pull-out specimens prepared according to ASTM D7913 [32] include a free end protruding bar, the impact of which has yet to be fully addressed in the literature. This study comprehensively examines the effect of free end bar protrusion on the GFRP bar-concrete bond behavior, which was not considered in the literature. A total of 56 pull-out specimens are cast using two different batches of concrete. The two concrete batches are distinguished as a high-strength concrete batch and a low-strength concrete batch. Two GFRP bar surface conditions are examined: one with a lacquer finish (identified by L in the name of the specimens) and another without any lacquer (identified by UL in the name of the specimens). Two free end conditions are studied: one with a free end protruded bar and one without any protrusion. Additionally, three bonded lengths are investigated, i.e., $5d_b$, $10d_b$, and $20d_b$, where d_b is the nominal bar diameter. The results are analyzed in terms of applied load versus loaded end slip or free end slip (for low strength concrete batch only). Bond strength [32] is computed and discussed considering the different influencing factors mentioned above. In total, 19 notched beams are prepared from the high-strength concrete batch and tested in a TPB setup to investigate the GFRP bar-concrete bond behavior, including both types of bar surface finishings. Digital image correlation (DIC) is used to obtain full-field displacement and strain fields. Using the DIC data and cross-sectional analysis, the force in the GFRP bar and the slip in notched beams are obtained. Finally, the GFRP bar force-slip responses from notched beams are compared to the applied load versus loaded end slip responses of pull-out tests. The results obtained provide an insight into the short-term bond behavior of the bars studied. Although the available literature indicated that exposure to acid, alkaline, and saline environments only marginally affected the bond behavior of composite bar-concrete pull-out specimens [19], further tests should be performed to assess the long-term bond behavior of the bars considered in this study.

2. Experimental campaign

In this Section, the mechanical properties of concrete and GFRP bars are described. The geometrical dimensions and preparation of the specimens for pull-out tests and TPB tests are explained. Finally, the test setups and procedures are presented.

2.1. Material properties

The GFRP bar used in the experimental campaign was featured with helical lugs, with a lug net spacing of 5.4 mm (Fig. 1). In the U. S. system, the bars are categorized as size #4. The nominal diameter (d_b) of the bars was 12 mm. The bar was manufactured using vinylester resin and E-CR glass, with a minimum fiber mass content of 75 %. Although all the bars were manufactured in the same manner, they were differentiated by their surface conditions. The bars were divided into two types: one was coated by the manufacturer with an exterior lacquer coating and the other was uncoated. In Fig. 1, the two surface conditions are discernible. The lacquered (L) bar shows a glossy finish due to the applied coating, while the unlacquered (UL) bar has a flat finish. The geometric and mechanical properties of the GFRP bars can be found in Table 1, as provided by the manufacturer [44]. The diameter reported in Table 1 was computed from the bar cross-sectional area (A_b) obtained according to Ref. [45].

The tensile strength of the unlacquered bars was also determined by the authors. The details of the GFRP bar tensile tests can be found in Ref. [28]. The average tensile strength for the unlacquered bars was equal to 977 MPa.

Two different concrete batches were used to cast the specimens. The concrete batches differed by their strength. The two batches of concrete are named Batch A and Batch B in the remainder of the paper. The pull-out test specimens and cylinders for material characterization were cast from both batches. The beams for the TPB tests were only cast from concrete Batch A. The concrete mix proportions were (water, cement, fly ash, fine aggregate, and coarse aggregate): 1.0:2.7:0.7:10.7:11.1 and 1.0:2.4:0.6:7.7:9.1 for Batch A and Batch B, respectively. Type I portland cement and Carey limestone were used. The maximum aggregate size was 10 mm for both batches of concrete. Specimens were covered with a plastic sheet after the casting process was completed and until demolding, which occurred 24 h later. Subsequently, the specimens were placed in a curing room for 28 days. The curing room maintained a temperature and relative humidity of 21 °C and 99 %, respectively. The curing process was same for all the beams and pull-out specimens.

Concrete compressive and splitting tensile strengths were determined per ASTM C39 [46] and ASTM 496 [47], respectively. These tests were performed on 150 mm (diameter) × 300 mm (height) concrete cylinders. The average compressive strength ($\bar{f}_c$) was determined at different ages (days from casting), using three specimens for each age, and is plotted in Fig. 2a, for both batches of concrete. Similarly, Fig. 2b shows the average splitting tensile strength ($\bar{f}_t$), also obtained from three specimens, across different concrete ages for both batches of concrete. It should be mentioned that the curing process for the cylinders used for material characterization of the concrete was same as the beams and cylinders as discussed above. At 28 days, concrete Batch A showed an average compressive strength of 40.3 MPa, while Batch B showed 27.8 MPa. Henceforth, Batch A is referred to as the *high-strength* concrete batch, and Batch B as the *low-strength* concrete batch.

2.2. Specimen preparation

The pull-out specimens consisted of a GFRP bar embedded in a concrete cylinder (Fig. 3). However, in six specimens, the bar was embedded in a concrete cube, following ASTM D7913 [32] standard. The purpose of testing cubic pull-out specimens was to verify that there was no influence of the shape of the concrete specimen on the test results. Pull-out specimens, cast from both concrete batches, were fabricated using lacquered (L) and unlacquered (UL) GFRP bars. Additionally, specimens with varying bonded lengths (ℓ) were investigated for both batches of concrete. These bonded lengths were chosen as multiples of the nominal bar diameter (d_b). From Batch A concrete, 34 pull-out specimens were cast, featuring bonded lengths of $5d_b$, $10d_b$, and $20d_b$. Among these, five were cubic pull-out specimens ($\ell = 5d_b$). Batch B concrete was used to cast 22 pull-out specimens, predominantly comprising $5d_b$ and $10d_b$ specimens. Batch B included one $20d_b$ bonded length specimen and one cubic pull-out specimen with $\ell = 5d_b$. The concrete cylinder of the pull-out specimens had a diameter of 200 mm. The bar, with a protruded part of 40 mm at the free end, was inserted into the cylinder with a bond breaker of 140 mm at the loaded end. Prior to testing, the protruded part of the bar was cut flush with the concrete surface for some pull-out specimens, to study the effect of the absence of the protruded bar at the free end. Additional details of the pull-out specimen preparation can be found in Refs. [28,48].

A total of 19 notched beams were tested in a TPB test setup (Fig. 4). Among these, ten notched beams had a nominal width (B) of 75

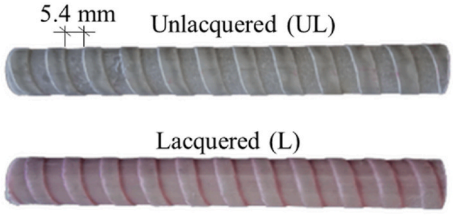

Fig. 1. GFRP bars used in the experimental study.

Table 1
GFRP bar geometric and mechanical properties as per manufacturer [44].

GFRP bar type	Diameter, (mm)	Area, A_b (mm^2)	Elastic modulus, E_b (GPa)	Tensile strength, f_b^* (MPa)
Lacquered (L)	13.2	137	64.2	1096
Unlacquered (UL)	13.5	144	62.5	1155

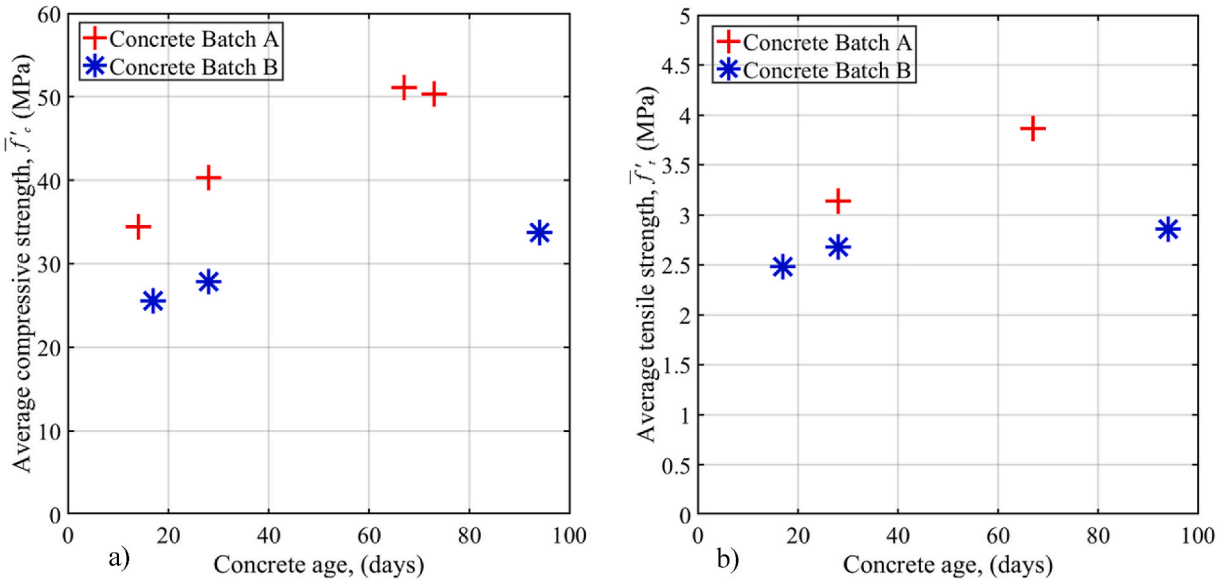

Fig. 2. Concrete material characterization: a) average concrete compressive strength versus the concrete age; and b) average concrete tensile strength versus the concrete age.

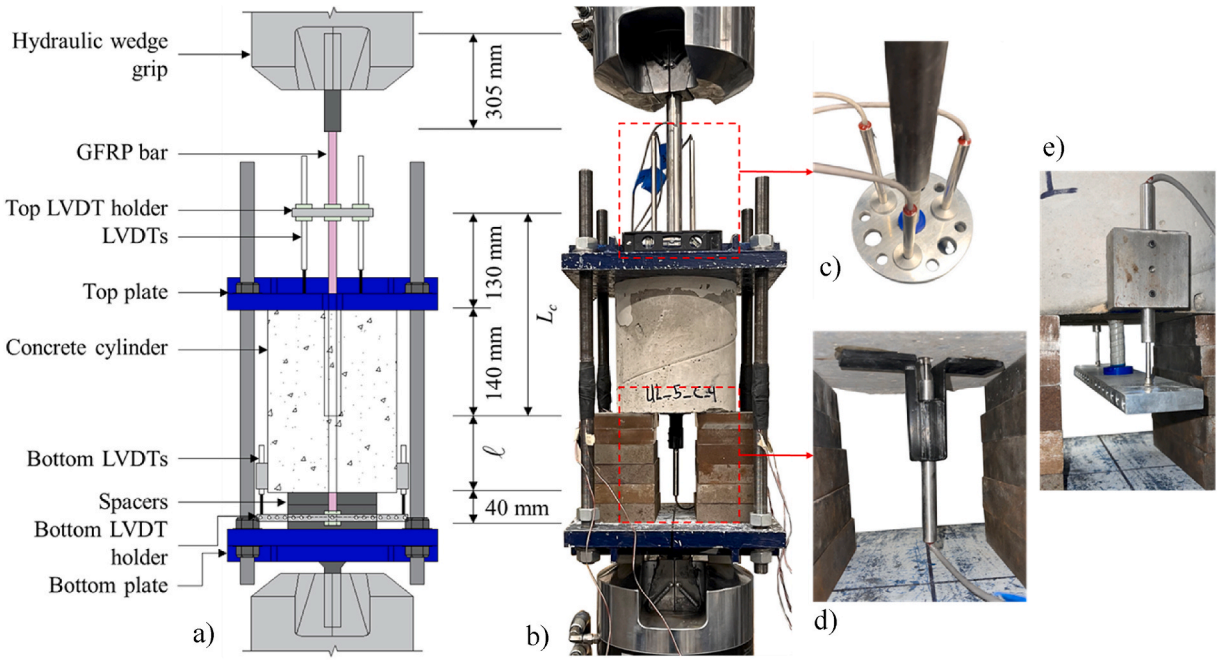

Fig. 3. Pull-out test setup: a) schematic of the test setup; b) photo of the real test setup; c) fixture used to measure the loaded end slip (g) using three LVDTs; d) fixture used to measure the free end slip (δ) using one LVDT; and e) fixture used to measure the free end slip (δ) using two LVDTs.

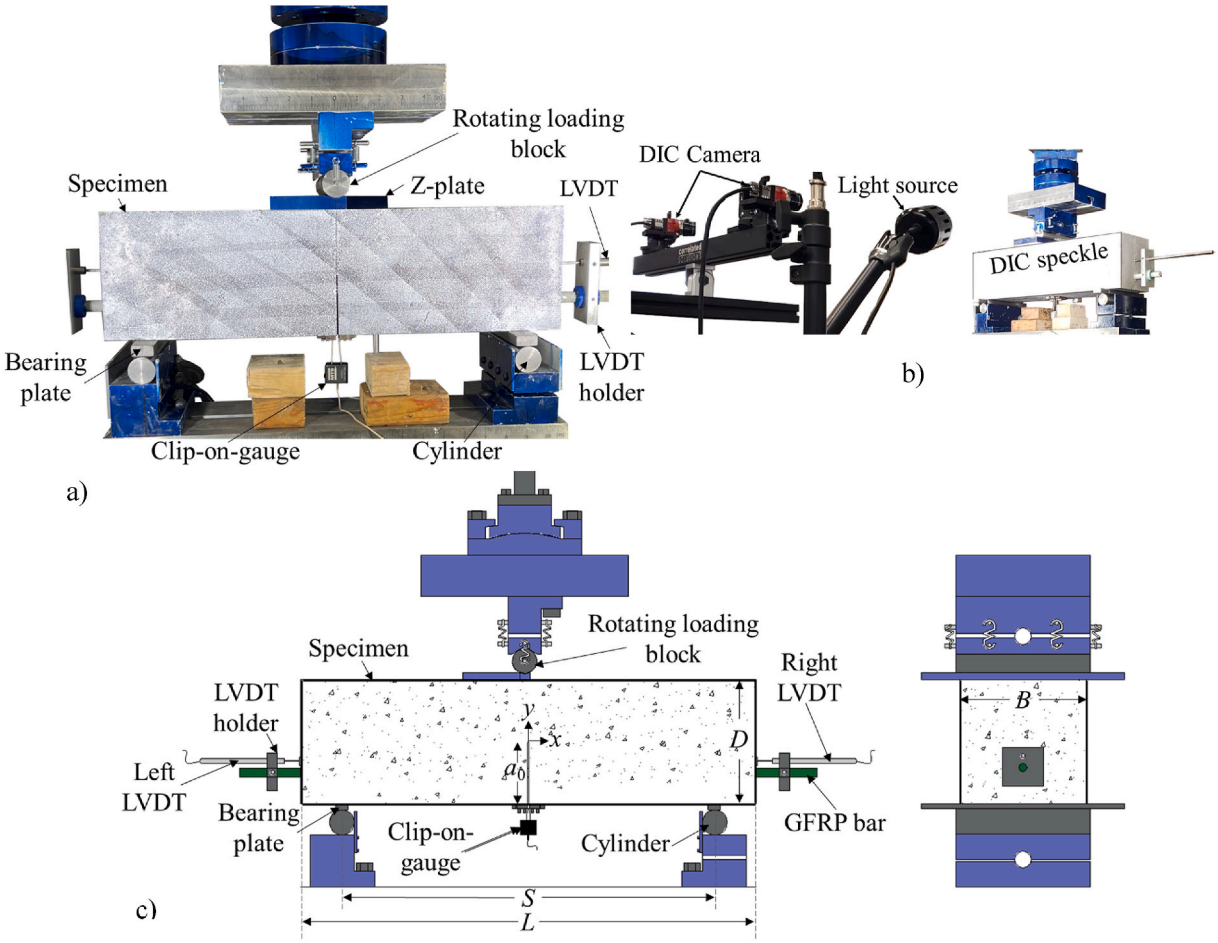

Fig. 4. Three-point bending test setup: a) actual photo of a test specimen; b) DIC setup; and c) a schematic of the test setup.

mm, while the remaining nine had a nominal width of 150 mm. When the bond failure is associated with concrete damage, there might be splitting of the concrete itself due to the radial stresses that arise from the interfacial stress transfer, especially when ribbed bars are used. To explore the case of a smaller amount of concrete on the side, two different widths of the beams were considered. The notched beams had some common nominal dimensions: nominal depth (D) of 150 mm, length (L) of 550 mm, loading span (S) of 450 mm ($=3D$), and initial notch length (a_0) of 75 mm, with a notched width (l) of 3 mm. Fifteen beams out of 19 were reinforced with either a lacquered (L) or unlacquered (UL) GFRP bar. The GFRP bar was positioned at the mid-width of the specimen and the distance between the centroid of the bar cross-section and the bottom face of the beam was 38 mm. Within this group, four beams were wrapped with a carbon fiber-reinforced polymer (CFRP) sheet on both sides of the initial notch to prevent shear failure. Four notched beams were cast as plain concrete without any reinforcement. The beam size was determined according to the draft of the ACI/ASCE 446 Technical Committee report, a guideline previously utilized by the authors [43,49]. Further details regarding the beam design are available in Ref. [43]. The choice of a depth (D) of 150 mm for the notched beams resembled that of specimens employed in traditional fracture mechanics tests and referenced in ASTM C293 [50], which determines the modulus of rupture of concrete. For GFRP bar reinforced concrete notched beams (briefly named *GFRP-RC notched beams*), the notches were cast, while unreinforced beams had their notches saw-cut with a V-shaped tip diamond blade. The GFRP bars were extended beyond the beam ends, allowing for displacement measurement at both ends using LVDT holders mounted onto these extended portions. Specific details about the casting process for the notched beams can be found in Ref. [43]. Nine GFRP-RC notched beams (using both L and UL bar) were prepared for DIC. This involved applying a speckle pattern onto one of the beam side faces, as shown in Fig. 4b. Before testing the specimens, the dimensions D, B, and L of the notched beams were measured at three different locations.

2.3. Test setup and procedure

2.3.1. Pull-out test

The experimental setup of pull-out tests, in accordance with ASTM D7913 [32] standard, involved restraining the specimen between two steel plates. These plates, designated as the top and bottom plates, were connected by four steel rods (Fig. 3a and b). To

measure the displacement at the loaded end (g) of the bar, three linear variable displacement transformers (LVDTs) were used (Fig. 3c). The displacement (δ) of the free end of the bar was measured for Batch B-concrete specimens only. In cases where the bar was cut flush with the concrete surface at the free end, a 3D printed plastic support for an LVDT was used to measure the free end slip (δ) of the bar (Fig. 3d). Alternatively, for specimens with a protruding bar at the free end, either one LVDT or two LVDTs were used to measure δ. In the case of one LVDT, the same holder mentioned above was used and the tip of the LVDT was reacting against the end cross-section of the bar. In the case of two LVDTs, two aluminum holders were glued to the concrete surface near the free end. The LVDTs reacted against an aluminum plate attached to the free end of the bar (Fig. 3e).

A thin layer of self-leveling mortar was applied to the concrete cylinder top surface to ensure a flat surface in contact with the top plate of the test setup. The pull-out tests were performed on a servo-hydraulic testing machine with a 250 kN capacity. To facilitate gripping of the bar by the servo-hydraulic testing machine jaws, a steel hollow cylinder (length = 305 mm, and diameter = 25.4 mm) was used at the top end of the bar. The test was displacement controlled at rate of 0.88 mm/min. The average (ξ) of the displacements measured by the top three LVDTs was used to control the test. Additional details regarding the experimental arrangement and test protocol can be found in Ref. [28].

2.3.2. Three-point bending (TPB) test

The test setup for the TPB tests is shown in Fig. 4. Two steel support cylinders were positioned apart to create the loading span ($S = 3D$) for the notched beams. An additional cylinder was placed at the mid-span to apply the load. The crack mouth opening displacement (CMOD) was measured using a clip-on gauge attached to the bottom edges of the notch. Steel blocks acting as bearing plates were affixed to the bottom of the beams and positioned on top of the support cylinders to minimize friction. This TPB test setup configuration was adapted from the draft of the ACI/ASCE 446 Technical Committee report, which was also used in previous studies [43,49].

The TPB tests were performed in CMOD control (except for CFRP-wrapped reinforced notched beams that were controlled by machine stroke) using the same servo-hydraulic universal testing machine of the pull-out tests. For CFRP-wrapped specimens, failure of the GFRP bar in tension was expected and the clip-on gauge used to measure the CMOD would have been damaged. The initial CMOD rate was chosen to reach the peak load (F_{max}) of the first ascending branch in the load response of the beams within a timeframe of 150–210 s. The unreinforced notched beams began with a CMOD rate of 0.0002 mm/s. This rate was increased to 0.0005 mm/s when the load reached 85 % of F_{max} in the descending portion of the response (softening branch). Finally, the CMOD rate was further increased to 0.001 mm/s upon reaching 35 % of F_{max} in the descending portion of the response. For the GFRP-RC notched beams the initial CMOD rate was 0.0002 mm/s. Once the first peak load (F_{max}) or the initial change in slope was identified, the CMOD rate was adjusted to 0.001 mm/s within the CMOD range of 0.15 mm–0.24 mm. Additionally, as the CMOD reached between 0.50 mm and 1.00 mm, the CMOD rate was further increased to 0.01 mm/s. A change in the CMOD rate was necessary to achieve approximately a constant strain rate at the tip of the propagating crack. The GFRP-RC notched beams wrapped with CFRP were tested in stroke control. The stroke rate was 0.015 mm/s. For unreinforced notched beams, the test was stopped when the load was between 3 % and 5 % of F_{max}. For GFRP-RC notched beams without CFRP wrap, the test ended when shear failure occurred, while when the GFRP-reinforced beams were wrapped with CFRP the test ended when the notch ligament was completely fractured, and bar fiber rupture occurred.

Table 2
Summary of the pull-out test specimens.

Pull-out Test Nomenclature: X_Y_Z_Q_(ASTM)						
X = Type of GFRP bar used; Lacquered (L) or Unlacquered (UL)						
Y = Bonded length (⁄); expressed as multiple of bar diameter (d_b)						
Z = Free end bar condition; C if free end bar is cut and P if free end bar is not cut						
Q = Number of specimen in each series; ASTM = If present, the specimen shape is cubic (ASTM 7913 [32])						
Series	X	Y	Z	Number of replicates	Number of replicates	Specimen shape
				Batch A	Batch B	
L_5_C_Q	L	$5d_b$	C	3	2	Cylinder
L_5_P_Q	L	$5d_b$	P	4	3	Cylinder
L_10_C_Q	L	$10d_b$	C	3	3	Cylinder
L_10_P_Q	L	$10d_b$	P	0	1	Cylinder
L_20_C_Q	L	$20d_b$	C	1	0	Cylinder
L_20_P_Q	L	$20d_b$	P	3	0	Cylinder
UL_5_C_Q	UL	$5d_b$	C	3	3	Cylinder
UL_5_P_Q	UL	$5d_b$	P	4	2	Cylinder
UL_10_C_Q	UL	$10d_b$	C	3	3	Cylinder
UL_10_P_Q	UL	$10d_b$	P	0	3	Cylinder
UL_20_C_Q	UL	$20d_b$	C	2	0	Cylinder
UL_20_P_Q	UL	$20d_b$	P	3	1	Cylinder
L_5_P_Q_ASTM	L	$5d_b$	P	3	0	Cube
UL_5_P_Q_ASTM	UL	$5d_b$	P	2	1	Cube

3. Experimental results of the pull-out tests

The nomenclature used for the pull-out tests follows the format X_Y_Z_Q. X is either equal to L (lacquered) or UL (unlacquered), indicating the type of GFRP bar used. Y denotes the bonded length (ℓ) as a multiple of the nominal diameter (d_b). For instance, when Y = 5, it indicates a bonded length of $5d_b$. Z indicates the free end bar condition. Z is equal to C when the protrusion of the bar was cut flush with the concrete surface, or Z is equal to P for specimens featuring the bar protrusion. Lastly, Q represents the number of specimen sharing the same type of bar (L or UL), bonded length (ℓ), and free end condition (C or P). The cubic pull-out test specimens are distinguished by adding "ASTM" at the end of their name. Table 2 summarizes the nomenclature of all pull-out specimens and the number of specimens tested. Tables 3 and 4 show the names of the tested specimens from Batch A and Batch B concrete, respectively. These tables also include the concrete age at the time of testing (counting from the day of casting), the failure mode, peak load (P^*), average peak load ($\overline{P}^*$), along with the coefficient of variation (CoV) for each group of specimens, and the bond strength (τ^*). The bond strength (τ^*) was computed as defined in ASTM 7913 [32]:

$$\tau^* = \frac{P^*}{\pi d_b \ell} \tag{1}$$

It should be noted that for some bonded lengths, and surface and protrusion conditions only one or two specimens were tested. The effect of the protrusion was observed after the specimens were cast and some replicates were cut to obtain specimens without the protrusion. The low CoV for group of specimens with 3 or more specimens encouraged the authors to consider reliable those tests without sufficient replicates.

3.1. Applied load P versus the loaded end slip g for all specimens

The load responses for all the specimens from both batches of concrete are shown in Fig. 5 in terms of applied load (P) versus the loaded end slip (g). The loaded end slip (g) was computed by subtracting the GFRP bar elongation from the average displacement of the three LVDTs (ξ) at the top

Table 3
Specimen geometry and experimental results for the pull-out tests cast from Batch A concrete.

Specimen	ℓ (mm)	Age of concrete when tested (days)	Failure mode	P^a (kN)	$\overline{P}^*$ (kN) [CoV]	τ^* (MPa)
L_5_C_1	60	76	Slippage	25.1	21.8 [0.13]	10.1
L_5_C_2	60	125	Slippage	18.0		7.2
L_5_C_3	60	125	Slippage	22.2		8.9
L_5_P_1	60	70	Slippage	53.6	53.0 [0.03]	21.5
L_5_P_2	60	94	Slippage	50.2		20.2
L_5_P_3	60	101	Slippage	54.8		22.0
L_5_P_4	60	101	Slippage	53.2		21.4
L_10_C_1	120	63	Slippage	64.6	66.8 [0.06]	13.0
L_10_C_2	120	103	Slippage	63.2		12.7
L_10_C_3	120	103	Slippage	72.6		14.6
L_20_C_1	240	125	Slippage	105.9	105.9	10.6
L_20_P_1	240	59	Bar rupture	137.6	136.5 [0.04]	13.8
L_20_P_2	240	61	Bar rupture	130.0		13.1
L_20_P_3	240	67	Bar rupture	142.0		14.3
UL_5_C_1	60	75	Slippage	21.9	22.9 [0.06]	8.6
UL_5_C_2	60	125	Slippage	21.8		8.6
UL_5_C_3	60	125	Slippage	25.0		9.8
UL_5_P_1	60	70	Slippage	53.8	55.0 [0.03]	21.1
UL_5_P_2	60	94	Slippage	57.6		22.7
UL_5_P_3	60	94	Slippage	55.2		21.7
UL_5_P_4	60	101	Slippage	53.6		21.1
UL_10_C_1	120	63	Slippage	57.6	61.1 [0.04]	11.3
UL_10_C_2	120	103	Slippage	64.2		12.6
UL_10_C_3	120	104	Slippage	61.6		12.1
UL_20_C_1	240	125	Slippage	103.5	106.0	10.2
UL_20_C_2	240	125	Slippage	108.5		10.7
UL_20_P_1	240	59	Bar rupture	137.3	139.3	13.5
UL_20_P_2[a]	240	61	Grip failure	124.3		12.2
UL_20_P_3	240	67	Bar rupture	141.3		13.9
L_5_P_1_ASTM	60	76	Slippage	50.8	52.5 [0.08]	20.4
L_5_P_2_ASTM	60	103	Slippage	48.5		19.5
L_5_P_3_ASTM	60	104	Slippage	58.3		23.4
UL_5_P_1_ASTM	60	76	Slippage	50.5	51.1	19.8
UL_5_P_2_ASTM	60	104	Slippage	51.8		20.4

[a] Specimen excluded from the computation of average peak load.

Table 4
Specimen geometry and experimental results for the pull-out tests cast from Batch B concrete.

Specimen	⁄ (mm)	Age of concrete when tested (days)	Failure mode	P^{a} (kN)	$\bar{P}^{*}$ (kN) [CoV]	τ^{*} (MPa)
L_5_C_1	60	105	Slippage	22.5	23.0	9.0
L_5_C_2	60	106	Slippage	23.6		9.5
L_5_P_1	60	101	Slippage	37.1	34.3 [0.06]	14.9
L_5_P_2	60	105	Slippage	32.1		12.9
L_5_P_3	60	107	Slippage	33.7		13.5
L_10_C_1	120	106	Slippage	47.6	50.0	9.6
L_10_C_2	120	119	Slippage	52.4		10.5
L_10_C_3[a]	120	106	Grip failure	42.2		8.5
L_10_P_1	120	107	Slippage	60.3	60.3	12.1
UL_5_C_1	60	101	Slippage	29.5	26.5 [0.08]	11.6
UL_5_C_2	60	105	Slippage	25.6		10.1
UL_5_C_3	60	106	Slippage	24.3		9.6
UL_5_P_1	60	105	Slippage	32.7	34.2	12.9
UL_5_P_2	60	107	Slippage	35.7		14.0
UL_10_C_1	120	119	Slippage	48.7	48.5 [0.02]	9.6
UL_10_C_2	120	119	Slippage	47.4		9.3
UL_10_C_3	120	119	Slippage	49.4		9.7
UL_10_P_1	120	107	Slippage	62.4	60.7 [0.04]	12.3
UL_10_P_2	120	108	Slippage	57.1		11.2
UL_10_P_3	120	108	Slippage	62.6		12.3
UL_20_P_1	240	109	Slippage	102.0	102.0	10.0
UL_5_P_1_ASTM	60	119	Slippage	31.5	31.5	12.4

[a] Specimen excluded from the computation of average peak load.

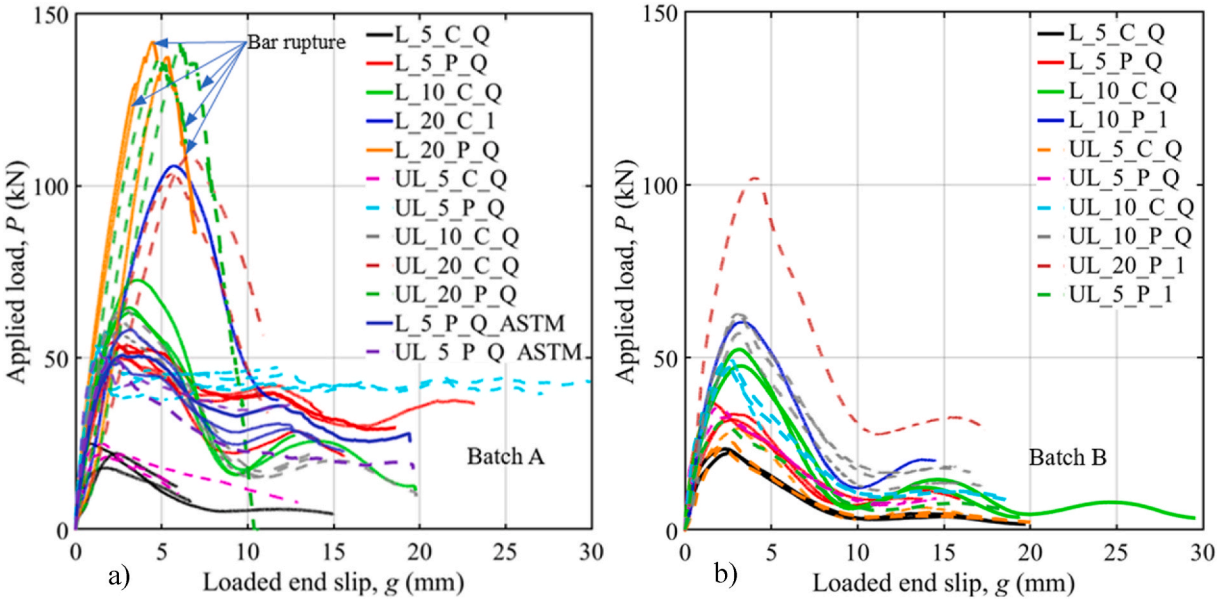

Fig. 5. Applied load (P) versus loaded end slip (g) for: a) Batch A concrete; and b) Batch B concrete.

$$g = \xi - L_c \varepsilon_b \tag{2}$$

where ε_b is the strain in the unbonded portion of the GFRP bar, which was determined by dividing the applied load by the product of cross-sectional area (A_b) and the elastic modulus (E_b) provided by the manufacturer for each type of bar [44] (see Table 1). $L_c = 270$ mm is the length of the segment of the bar between the beginning of the bonded area and the location where the LVDT holder was attached to the bar (Fig. 3). It should be mentioned that the readings of the three top LVDTs were consistent. Fig. 5a and b show the applied load (P) versus the loaded end slip (g) responses for all the pull-out tests cast from Batch A and Batch B concrete, respectively. The P-g responses from both batches have similar features: at the beginning of the test, the response is linear elastic followed by a brief non-linear part before attaining the peak load (P^{*}). The specimens in series L_20_P_Q and specimens UL_20_P_1 and UL_20_P_3 from Batch A concrete failed due to bar rupture. Their applied load versus loaded end slip responses were similar (in terms of initial stiffness and shape of the curve) to those of the other specimens. After the peak load is reached, the load decreases as g increases and the

response featured oscillations in the load. For Batch B specimens, the values of g corresponding to the peak and valley of the oscillation appear to be consistent.

In a previous study by the authors [28], similar load responses were observed for a different type of GFRP bar that had the same nominal diameter as the GFRP bars used in this study. However, in that study, the GFRP was sand coated with a helically wrapped carbon fiber bundle on the surface. The magnitude of the oscillations in the previous study [28] was not as significant as that observed in this study. In addition, the highest load during the first oscillation after P^* was similar in magnitude to P^* for few specimens in the previous study [28], which was not observed in this study. If the average peak loads $\overline{P}^*$ of L and UL specimens with the same bonded length from this study and the sand coated bars from the previous study are compared, it can be observed that the $\overline{P}^*$ for L and UL bars from both batches are higher compared to $\overline{P}^*$ of the sand coated bars (for example considering $\ell = 5d_b$, the average peak loads using L and UL bars from Batch A concrete are 284 % and 295 % higher than the average peak loads using sand coated bars in the previous study [28]). It should be noted that the concrete compressive strength in the previous study was 34 MPa at 28 days from the day of casting. Since the GFRP bars used in both studies had the same nominal diameter and similar tensile strength, these differences can be attributed to the surface conditions of the bar.

3.2. The effect of GFRP bar coating

To investigate the effect of GFRP bar surface coating, specimens from both concrete batches using L and UL bars that had the free end bar cut flush with concrete (i.e., C specimens) were selected and the P-g responses for those specimens are shown in Fig. 6. The reason for only considering C specimens is that the effect of protrusion could create an interference in the comparison. Fig. 6a shows the P-g responses for Batch A-concrete specimens. If the load responses of specimens with the same bonded lengths ($5d_b$, $10d_b$, and $20d_b$) and with L and UL bars are considered, the peak loads and the overall trend of the response are similar except for L_10_C_3, which had higher peak load compared to other L_10_C and UL_10_C specimens. The average peak load for L bar specimens with $5d_b$, $10d_b$, and $20d_b$ bonded lengths was 21.8 kN, 66.8 kN, and 105.9 kN. For UL bar specimens, the average peak loads were 22.9 kN, 61.1 kN, and 106.0 kN. The difference in peak loads between L bar and UL bar specimens was 1.1 kN for $5d_b$, 5.7 kN for $10d_b$, and 0.1 kN for $20d_b$ bonded length, which was deemed negligible. From Fig. 6b, which shows the same comparison between L and UL bars but for the Batch B-concrete specimens, it can be observed that there is no significant difference in peak loads and overall response trend between L and UL specimens except for L_10_C_2 and UL_5_C_1, which had higher peak loads compared to the other specimens of the same group. Fig. 6 shows that the peak and valley of the oscillation in different specimens occurs at a similar value of g regardless of the bar type and bonded length. This phenomenon was also observed in the previous study with sand coated bars [28].

3.3. The effect of concrete strength

The effect of concrete strength is discussed by comparing the responses of Batch A- ($\bar{f}_c{}' = 40.3$ MPa) and Batch B- ($\bar{f}_c{}' = 27.8$ MPa) concrete specimens. Fig. 7 shows the effect of concrete strength in pull-out tests considering only L bar specimens. To separate the effect of the bar protrusion from the effect of concrete strength, Fig. 7a and b show the P-g responses for L bar specimens for different

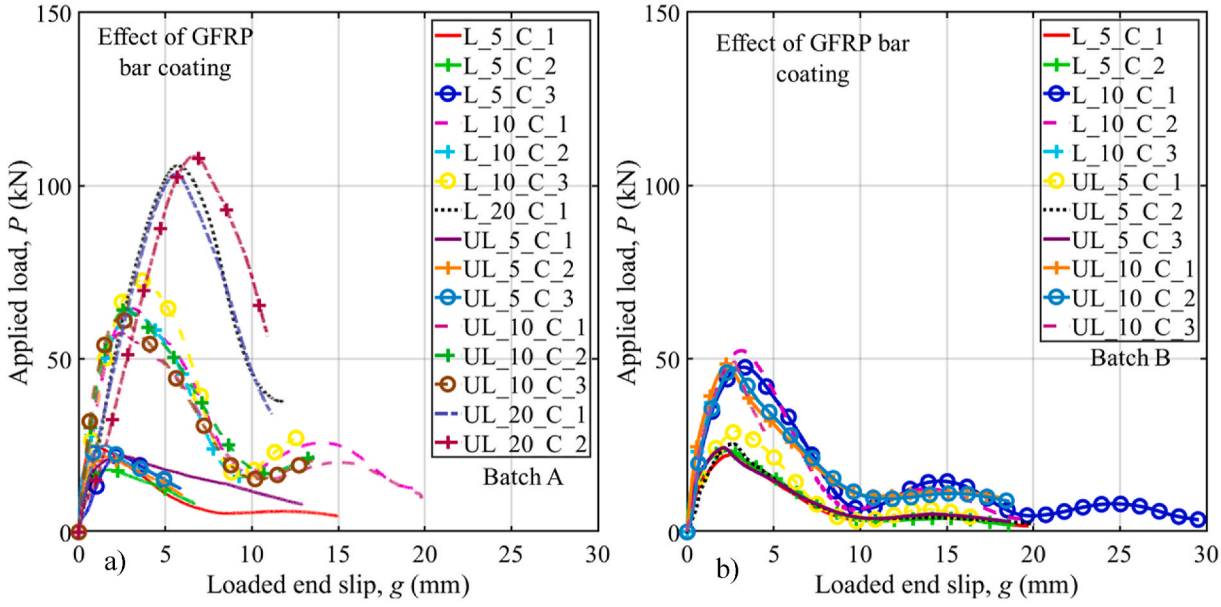

Fig. 6. Effect of GFRP bar coating for: a) Batch A-concrete specimens; and b) Batch B-concrete specimens.

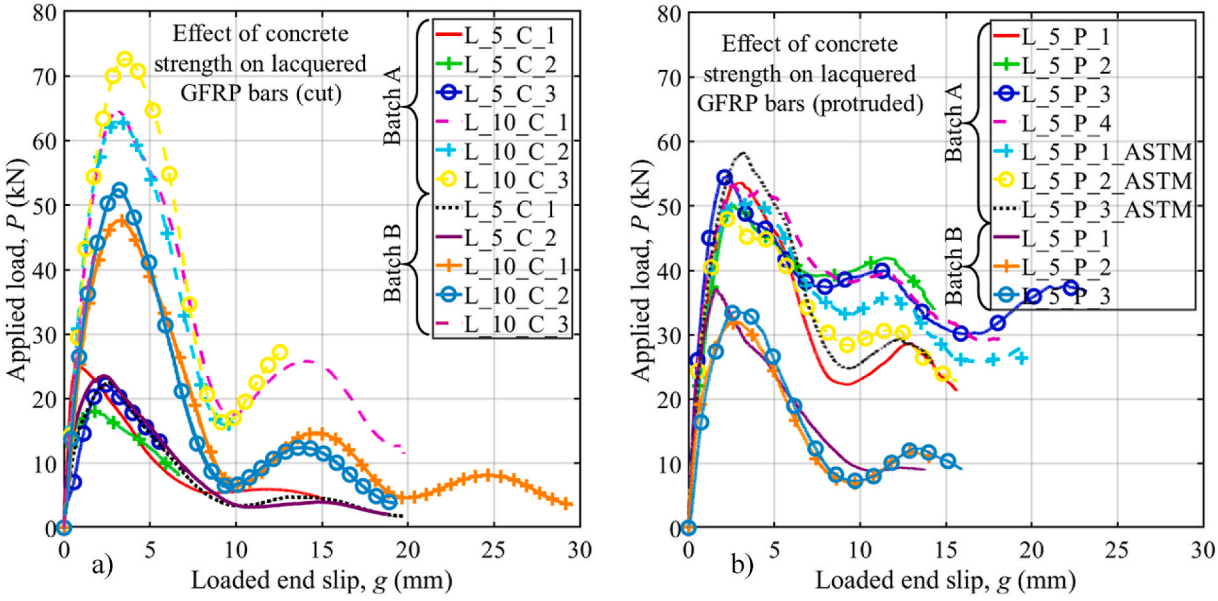

Fig. 7. Effect of concrete strength on specimens with lacquered GFRP bars: a) free end cut; and b) free end protruded bar.

bonded lengths without and with the free end protrusion, respectively. From Fig. 7a, the responses from both batches of concrete have similar features as described in the previous sections. In terms of peak loads, $\ell = 5d_b$ specimens from both batches show insignificant difference. However, for $\ell = 10d_b$ specimens, the average peak load for Batch A-concrete specimens was 66.8 kN, which is approximately 1.4 times the average peak load (47.4 kN) of Batch B-concrete specimens. It could be assumed that the smaller bonded length ($\ell = 5d_b$), having comparatively lesser contact area with the concrete than that of specimens with longer bonded length, might not be enough to reflect the effect of concrete strength. Fig. 7b only consists of $\ell = 5d_b$ specimens that have protruded L bar at free end. Again, the *P-g* responses have similar features, which do not vary with concrete strength. For Batch A-concrete cylindrical and cubic (ASTM) pull-out specimens, the average peak loads are approximately 1.5 times higher than the average peak load of Batch B-concrete cylindrical specimens ($\bar{P}^{*}$ = 34.3 MPa). Since the results of Fig. 7a suggested that the smaller bonded length might not be enough to reflect any effect of concrete strength on the peak load, the higher peak loads observed for Batch A-concrete $\ell = 5d_b$ specimens can be attributed to the presence of the protruded bar at the free end. It can be assumed that higher strength concrete (Batch A) showed higher

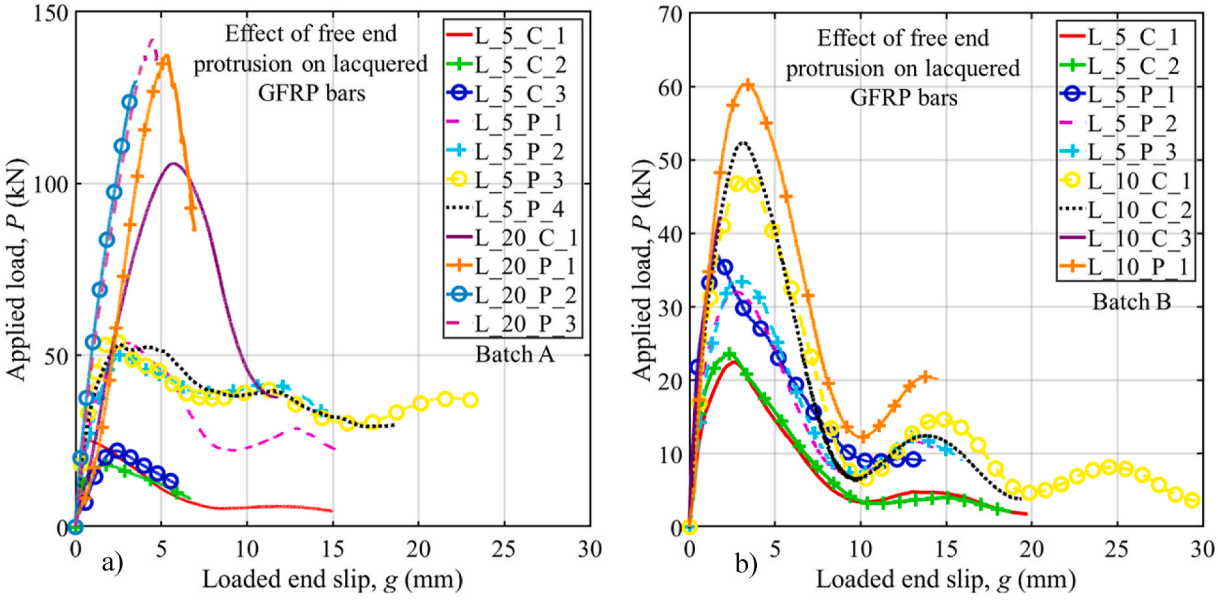

Fig. 8. Effect of free end protrusion for: a) specimens with lacquered (L) bars from Batch A concrete; and b) specimens with lacquered (L) bars from Batch B concrete.

resistance as the protruded bar at the free end was starting to move inside, whereas the lower strength concrete (Batch B) showed comparatively lesser resistance. Additional discussion on this point is provided in the next sub-Section.

The effect of concrete strength in the pull-out specimen tests with UL bars was similar to that described above for the L bars.

3.4. The effect of free end bar protrusion

Fig. 8a shows the effect of the free end bar condition, i.e., a comparison between protrusion (P) specimens and cut-flush (C) specimens, focusing on Batch A-concrete L bar specimens, with two different bonded lengths (i.e., $5d_b$ and $20d_b$). For specimens with $\ell = 5d_b$, $\overline{P}^*$ of C specimens was 21.8 kN, showing a 31.2 kN reduction compared to $\overline{P}^*$ of P specimens. In terms of overall load response features, no other significant differences were observed due to the presence of the free end bar protrusion. For $\ell = 20d_b$ specimens, the only C specimen exhibited a peak load of 105.9 kN, while $\overline{P}^*$ of P specimens was 136.5 kN, showing a 30.6 kN increase over the C specimen. This suggests that the presence of the protrusion contributed approximately 31 kN to the peak load, independently of the bonded length. It can be assumed that the protrusion acted as an anchor at the free end and the load difference between C and P specimens could be regarded as the load required to initiate the slippage of the protrusion inside the concrete. The *P-g* responses using Batch A-concrete UL bars specimens were also compared in terms of the effect of the protrusion and it was found that its effect was consistent across bonded lengths, and it did not seem to be influenced by the surface coating of the bar. Both L and UL bar specimens showed load differences of similar magnitude when C and P specimens were considered, as it can be inferred from Table 3.

Fig. 8b shows the effect of free end bar protrusion on Batch B-concrete specimens. In Fig. 8b, the *P-g* responses for L bar specimens with bonded lengths of $5d_b$ and $10d_b$ are reported. No significant differences were observed in the features of load responses due to the free end conditions. For C specimens with $\ell = 5d_b$, $\overline{P}^*$ was 23 kN, showing a reduction of 11.3 kN compared to $\overline{P}^*$ (=34.3 kN) for P specimens. In the case of $\ell = 10d_b$, the $\overline{P}^*$ was equal to 50.1 kN, which resulted 12.9 kN lower than P^* (=60.3 kN) of specimen L_10_P_1. Similarly to the results from Batch A-concrete specimens discussed above, the Batch B-concrete L specimens showed a consistent contribution to peak load due to the presence of the protrusion, regardless of the bonded length. Batch A-concrete specimens with L bars showed on average a higher gain in peak load (31 kN) compared to Batch B-concrete specimens with L bars (12.1 kN) due to the effect of free end bar protrusion. The protrusion acts like an anchor and therefore energy, i.e., additional load, is required for the protruded part to damage the surface of concrete at the free end and slip in. This energy is dependent on the properties of concrete and therefore concrete with a lower strength should have less resistance to the slippage of the protruded part into concrete. The *P-g* responses with UL bars from Batch B concrete was also investigated and similar results as the L bars were found, as it can be inferred from Table 4.

3.5. GFRP bar slip at the free end

The free end slip (δ) was measured for all Batch B-concrete specimens. Fig. 9 shows the *P*-δ responses for these specimens. When two LVDTs were used to measure the free end slip, the average value of both LVDTs was used as δ. At the beginning of the test, the free end slip was near zero, followed by a brief linear *P*-δ response. The linear response was followed by a nonlinear part that ultimately led to

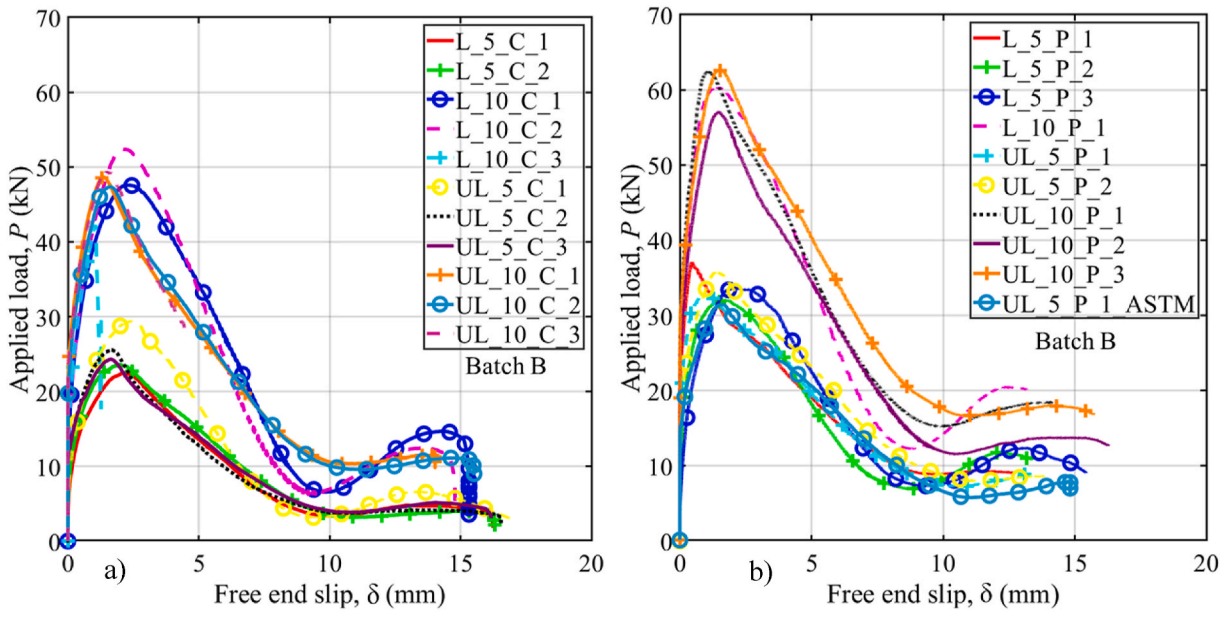

Fig. 9. Effect of bar surface coating on the free end slip for Batch B-concrete specimens: a) free end cut; and b) free end protruded.

the peak load (P^*). Following the peak load, the P-δ responses resembled the P-g responses, featuring an oscillating pattern. Similarly to the P-g responses, the peaks and valleys of the oscillations in P-δ also appeared to occur at consistent δ values. As the bonded length increased, the load at which a nonzero δ was observed also increased. Fig. 9 shows the effect of bar surface coating on the P-δ responses. In Fig. 9a, the P-δ responses are plotted for C specimens with $\ell = 5d_b$ and $\ell = 10d_b$. The $\ell = 5d_b$ specimens showed no remarkable influence of surface coating on P-δ responses. Similarly, the $\ell = 10d_b$ specimens showed no significant effect of surface coating. Fig. 9b shows the P-δ responses for P specimens. No substantial differences were identified between the responses of L bar specimens and UL bar specimens. As a confirmation of the anchor effect of the protruding part of the bar at the free end, it can be observed that the values of δ for the same bonded length, bar coating condition, and load magnitude are smaller for P specimens than for C counterparts. This is particularly evident when the ascending branches of the responses are compared.

3.6. Failure modes of pull-out tests

Most pull-out tests were stopped when substantial slippage between the GFRP bar and the concrete occurred. In Tables 3 and 4, this type of failure is denoted as "slippage". For Batch A-concrete specimens, irrespective of the coating condition (except for UL_20_P_2), when the bonded length was $20d_b$ and the specimen featured a protruded part at the free end, rupture of the bar was observed. This type of failure is labeled as "bar rupture" in Table 3 and it is shown in Fig. 10a. No Batch B-concrete specimen failed due to bar rupture. Furthermore, specimens UL_20_P_2 from Batch A concrete and L_10_C_3 from Batch B concrete exhibited slip between the cylindrical hollow grip and the bar, most likely due to an incorrect application of epoxy resin. These two specimens are categorized as "grip failure" in both Tables 3 and 4, and are excluded from the computation of the average peak loads. In a prior investigation involving sand-coated bars [28], pull-out tests (with protrusion at the free end) did not show bar rupture at $\ell = 20d_b$ (bar rupture occurred at $\ell = 40d_b$). In contrast, when using L or UL bars, bar rupture was achieved with $\ell = 20d_b$ (Batch A concrete), indicating a shorter bonded length needed to develop the stress transfer for L and UL bars compared to sand-coated bars. It should be noted that none of the pull-out specimens failed due to the splitting of the concrete cylinder. This is consistent with findings by Gravina et al. [51] that reported splitting failure likely occurs when the concrete cover-to-bar diameter ratio is smaller than 3.5.

Debris was observed on the bottom plate of the test fixture just beneath the protruded GFRP bar (Fig. 10b). Conversely, no debris was found in C specimens as the bar started slipping inside (Fig. 10c). As the protruded bar began to slip inside the concrete cylinder, the helical lugs started shearing off, resulting in debris of GFRP bar mixed with concrete debris. To investigate the bar and concrete interface, a few specimens from both batches of concrete were longitudinally cut open for microscopic analysis. Fig. 10d–g show the portion of the specimen cut open and its microscopy images for Batch A-concrete L_10_C_1 specimen. On the concrete surface

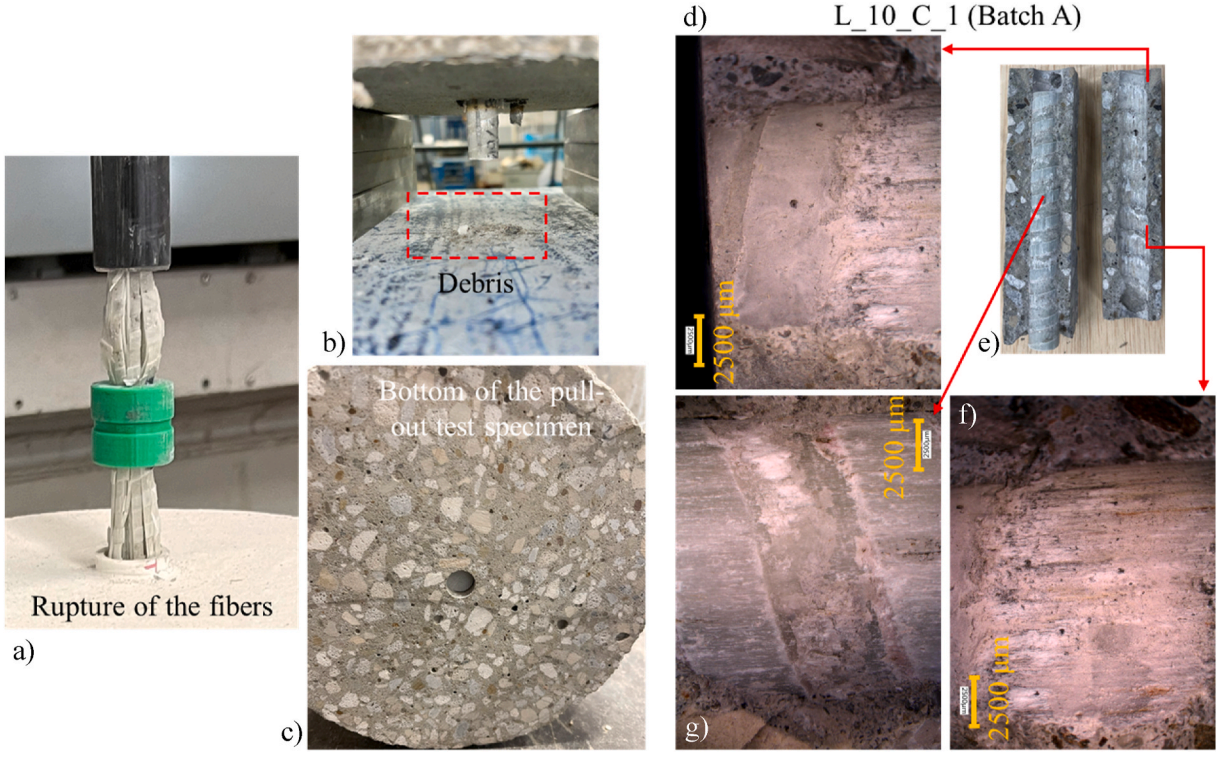

Fig. 10. Pull-out specimens after tests and microscopy images of L_10_C_1 from Batch A concrete: a) rupture of the bar fibers; b) accumulated debris on the bottom plate of the test fixture; c) bottom of the pull-out specimen with free end cut; d) impressions of bar helical lugs on concrete; e) photo of the cut open portion of the specimen; f) the lacquer coating found on concrete surface; and g) concrete between helical lugs of the bar.

(Fig. 10d), impressions of the helical lugs were found, along with remnants of the partially abraded helical lugs of the GFRP bar. The lacquer of the bar appeared to be removed by the concrete (Fig. 10e–f) as the bar slipped with respect to concrete. Additionally, Fig. 10g shows remnants of concrete between the helical lugs, which had undergone severe abrasion.

Fig. 11a–d show portion of the specimen cut open and its microscopic images for Batch A-concrete UL_5_P_1. In contrast to L_10_C_1 from the same batch, the bar surface appeared to be severely damaged (Fig. 11a–b).

The concrete sheared off the helical lugs, leaving white residue on the concrete surface (Fig. 11c). It can be assumed that the combined factors of the absence of lacquer coating and the high strength of the concrete contributed to the shearing off of the helical lugs (Fig. 11d). For comparison with Batch B-concrete specimens, Fig. 11e–g include the cut open portion of Batch B-concrete UL_5_P_1 specimen and its microscopy images. Despite featuring a protruded free end bar and no lacquer coating, the helical lugs on the surface did not appear to be sheared off but instead underwent partial abrasion only, with concrete residues present between the helical lugs (Fig. 11e–g). This phenomenon was attributed to the lower strength of the concrete. Therefore, the observed failure modes show the influence of concrete strength on the bond mechanism. This explains the different values of the peak load between Batch A- and Batch B-concrete specimens with the same bonded length and the presence of the protrusion at the free end. The different bond behavior attributed to mechanical properties of concrete should be studied including microstructure analysis of concrete, which was not carried out in this work.

3.7. Bond strength τ^* versus bonded length ℓ

Fig. 12a shows the bond strength (τ^*) for all pull-out specimens as a function of ℓ. The specimens in Fig. 12a are categorized based on concrete batch, surface coating, pull-out specimen geometry, and free end conditions. Generally, it can be observed that the bond strength within each group of specimens remains consistent. In Fig. 12b, the average bond strength ($\overline{\tau}^*$) for each group of specimens is shown as a function of ℓ. For Batch A-concrete specimens with $\ell = 5d_b$, both L and UL bars exhibit $\overline{\tau}^*$ approximately twice as high for P specimens compared to C specimens. A similar trend is observed for Batch B-concrete specimens with $\ell = 5d_b$, although the difference is not as large as for Batch A-concrete specimens, which indicates that the presence of the protrusion and the concrete strength affect the peak load. For Batch B-concrete $\ell = 10d_b$ specimens, a difference in $\overline{\tau}^*$ associated with the free end condition is present but less pronounced than that of specimens with $\ell = 5d_b$. For Batch A-concrete $\ell = 20d_b$ specimens, a similar trend is observed. In general, the difference in $\overline{\tau}^*$ between C and P specimens decreases as ℓ increases. However, the difference between C and P specimens has a different rate with increasing bonded length for Batch A- and Batch B-concrete specimens. For different groups of specimens, including Batch A-concrete L and UL specimens with bar protrusion, Batch B-concrete L and UL specimens with protrusion, and Batch B-concrete UL specimens without protrusion, $\overline{\tau}^*$ tends to decrease as the bonded length increases.

This observation aligns with a previous study on pull-out specimens with free end protruded bars [28]. Thus, specimens with free end protruded bars show a consistent behavior as bonded length increases, regardless of surface coating and concrete strength. From the remaining group of specimens, i.e., Batch A-concrete L specimens without protrusion and Batch A-concrete UL specimens without protrusion, $\overline{\tau}^*$ increases as ℓ increases from $5d_b$ to $10d_b$, followed by a decrease at $\ell = 20d_b$. A similar increasing pattern in bond

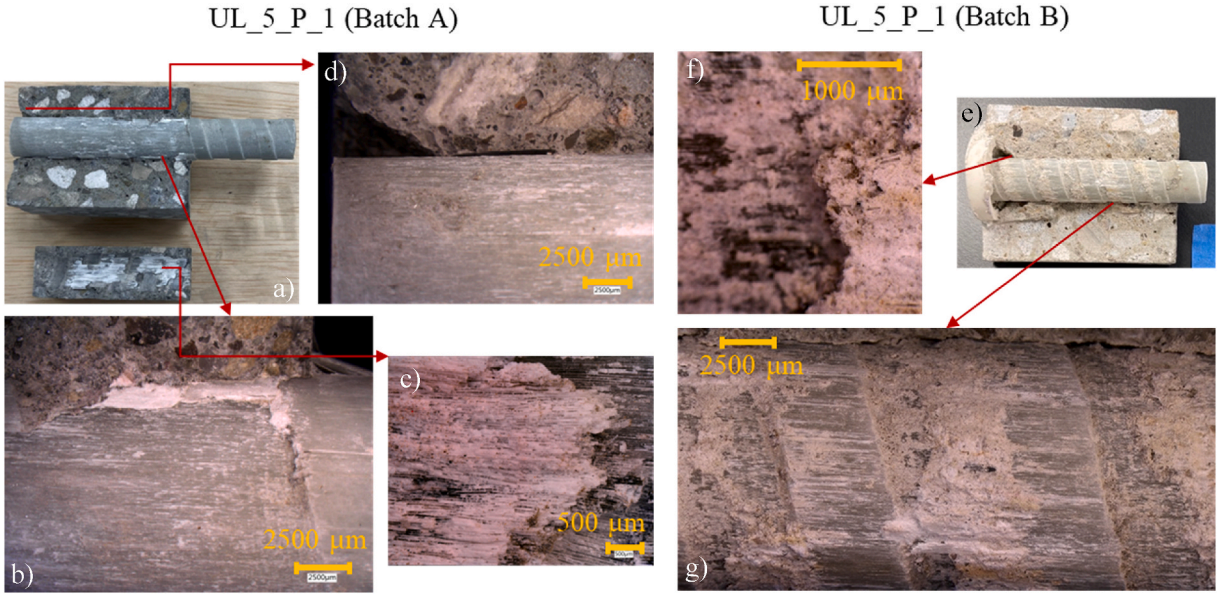

Fig. 11. Microscopy images of UL_5_P_1 from Batch A concrete: a) photo of the cut open portion of the specimen; b) scratched bar surface; c) white residue from sheared off helical lugs; and d) protruded free end condition. Microscopy images of UL_5_P_1 from Batch B concrete: e) photo of the cut open portion of the specimen; f) concrete residue in between helical lugs; and g) abraded helical lugs with concrete between them.

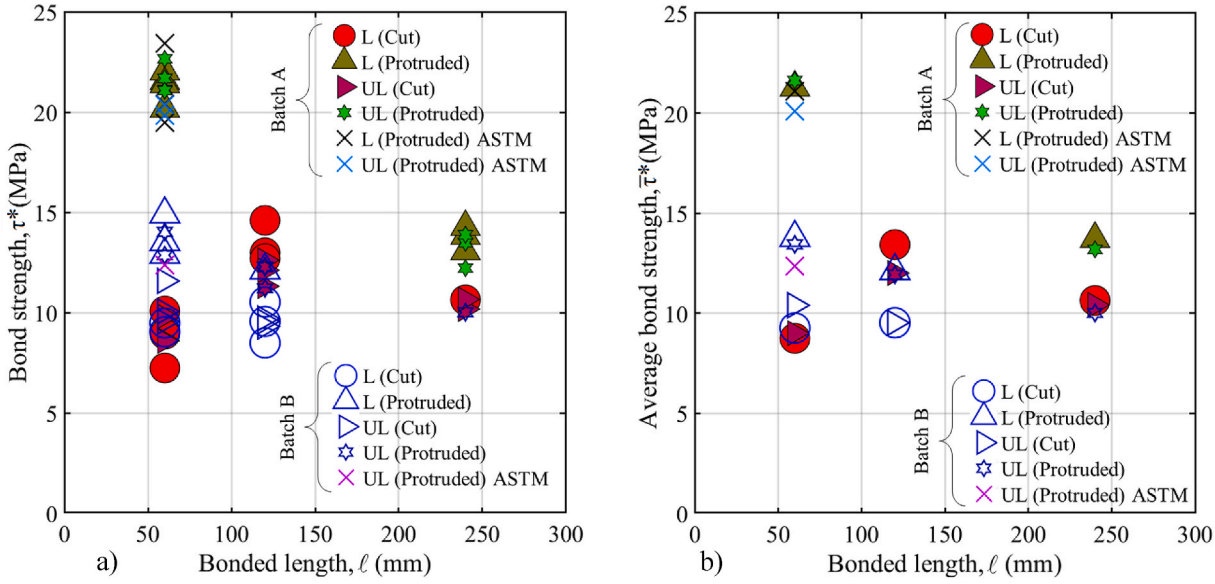

Fig. 12. a) GFRP bar-concrete bond strength versus bonded length including all the specimens from both batches of concrete; and b) average GFRP bar-concrete bond strength versus the bonded length for all specimens from both batches of concrete categorized in different groups of specimens.

strength is observed for Batch B-concrete L specimens without protrusion as the bonded length increases from $5d_b$ to $10d_b$. For Batch A-concrete ASTM specimens, which featured the bar protrusion, their $\bar{\tau}^*$ values were consistent with their corresponding cylindrical specimens with the same bar coating and $\ell = 5d_b$. Only one Batch B-concrete ASTM specimen was tested and while it might not be statistically significant, it was consistent with the corresponding cylindrical specimens as well.

4. Experimental results for the TPB tests

The experimental results of the 19 TPB tests on Batch A-concrete notched beams are reported in this section. The GFRP-RC notched beams were named NB_Z_Y_X, where Z is either L or UL and identifies if the beam was reinforced with either a lacquered bar (L) or an unlacquered bar (UL). Y denotes the width of the specimen in inches, which was either 3 inches or 6 inches. Thus, Y is equal to 3 (i.e., $B = 75$ mm) or 6 (i.e., $B = 150$ mm). X denotes the number of the beam within each group. The NB is used as an acronym for notched beams. The GFRP-RC beams that were wrapped with CFRP were identified with a W at the end of their name, i.e., NB_Z_Y_X_W, where W is used to indicate wrapped. The unreinforced concrete specimens were named NB_Y_X_P, where P is used to indicate plain specimens and Y and X are defined above. Table 5 summarizes the nomenclature of all notched beam specimens and the number of specimens tested. Table 6 shows the average measurements of notched beam depth (D), width (B), and length (L) along with their coefficient of variation (CoV) expressed as a percentage. Additionally, the initial notch length (a_0) and the weight of each specimen are

Table 5
Summary of notched beam specimens.

Notched Beam Test Nomenclature NB_Z_Y_X_(W)_(P)					
Z = Type of GFRP bar used; Lacquered (L) or Unlacquered (UL)					
Y = Beam width in inches (3" = 75 mm or 6" = 150 mm)					
X = Number of specimen in each series					
W = If presents, indicates CFRP wrapped specimens					
P = If presents, indicates plain concrete specimens					
Series	Z	Y	Number of replicates	W	P
NB_L_3_X	L	3	4	No	No
NB_L_6_X	L	6	1	No	No
NB_L_6_X_W	L	6	3	Yes	No
NB_UL_3_X	UL	3	4	No	No
NB_UL_6_X	UL	6	2	No	No
NB_UL_6_X_W	UL	6	1	Yes	No
NB_3_X_P	N/A	3	2	No	Yes
NB_6_X_P	N/A	6	2	No	Yes

Table 6
– Geometrical properties of the notched beams and experimental results.

Specimen	D (mm) [CoV (%)]	B (mm) [CoV (%)]	L (mm) [CoV (%)]	S (mm)	Weight (N)	a_0 (mm)	F_{max} (kN)	$\overline{F}_{max}$ (kN) [CoV]
NB_L_3_1	154.8 [0.3]	79.5 [1.9]	562.4 [0.2]	457.2	166.4	76.2	5.8	5.2 [11.6]
NB_L_3_2	153.4 [0.2]	78.2 [0.3]	467.2 [3.4]	457.2	161.5	76.2	5.1	
NB_L_3_3	153.5 [0.3]	78.2 [0.3]	560.3 [0.3]	457.2	160.7	76.2	5.5	
NB_L_3_4	153.3 [0.3]	78.4 [0.5]	560.3 [0.3]	457.2	161.1	76.2	4.4	
NB_L_6_1	161.3 [4.7]	156.4 [0.8]	561.3 [0.2]	457.2	305.8	76.2	8.3	8.3 [-]
NB_L_6_1_W	153.4 [0.2]	154.4 [0.2]	560.9 [0.7]	457.2	308.9	76.2	10.1	9.1 [10.0]
NB_L_6_2_W	153.7 [0.4]	154.4 [0.3]	559.8 [0.3]	457.2	308.7	76.2	8.7	
NB_L_6_3_W	153.2 [0.3]	153.4 [0.7]	559.8 [0.3]	457.2	308.4	76.2	8.4	
NB_UL_3_1	154.7 [0.2]	78.2 [1.1]	561.8 [0.3]	457.2	157.0	76.2	–	–
NB_UL_3_2	153.5 [0.3]	78.2 [0.3]	562.4 [0.2]	457.2	162.1	76.2	–	
NB_UL_3_3	153.4 [0.2]	78.5 [0.6]	559.3 [0.2]	457.2	160.9	76.2	–	
NB_UL_3_4	153.5 [0.3]	78.2 [0.3]	560.3 [0.3]	457.2	161.1	76.2	–	
NB_UL_6_1	151.7 [0.2]	161.9 [8.2]	561.8 [0.0]	457.2	311.6	76.2	12.2	11.9 [3.6]
NB_UL_6_2	153.4 [0.2]	154.4 [0.2]	561.3 [0.0]	457.2	313.0	76.2	11.6	
NB_UL_6_1_W	154.5 [0.5]	152.7 [0.2]	558.8 [0.0]	457.2	306.7	76.2	13.6	13.6
NB_3_1_P	153.4 [0.2]	78.2 [0.2]	558.8 [0.0]	457.2	157.8	76.2	5.1	4.9 [5.8]
NB_3_2_P	153.3 [0.3]	78.2 [0.9]	558.8 [0.0]	457.2	158.8	76.2	4.7	
NB_6_1_P	154.0 [0.5]	153.2 [1.4]	558.8 [0.0]	457.2	310.9	76.2	9.6	9.2 [6.9]
NB_6_2_P	152.7 [0.5]	154.3 [0.3]	558.8 [0.0]	457.2	308.7	76.2	8.7	

reported in Table 6. Table 6 also shows the first peak loads (F_{max}) for all specimens and the average first peak loads ($\overline{F}_{max}$) for each group of specimens along with their CoV (%). It should be mentioned that for the GFRP-RC notched beams, the first peak load F_{max} in Table 6 is identified as the load point before the start of the descending (softening) part or that where the first change of slope occurred. If the change in slope was not clearly identified, F_{max} is not reported in Table 6. All TPB tests were performed between 109 and 123 days from the day of casting.

4.1. Applied load versus stroke

Fig. 13a shows the load responses for all notched beams tests in terms of applied load (F) versus machine stroke. Fig. 13b is a call-out of the first part of the responses of Fig. 13a. Fig. 13a shows that in terms of load carrying capacity the CFRP-wrapped specimens reached greater loads than specimens without the CFRP wrap. The flexural load-carrying capacity of GFRP-RC notched beams without CFRP wrap was not attainable, as those specimens failed by concrete shear failure, which is not considered a desirable failure mode in this study. All the GFRP-RC notched beams show an initial linear response followed by a transition segment defined by a change of slope or brief descending portion of the response. The second portion of the response is pseudo-linear. For some of the GFRP-RC notched beams that were not CFRP-wrapped, such as NB_L_3_4, NB_UL_6_1, and NB_UL_6_2, the end of the response features a

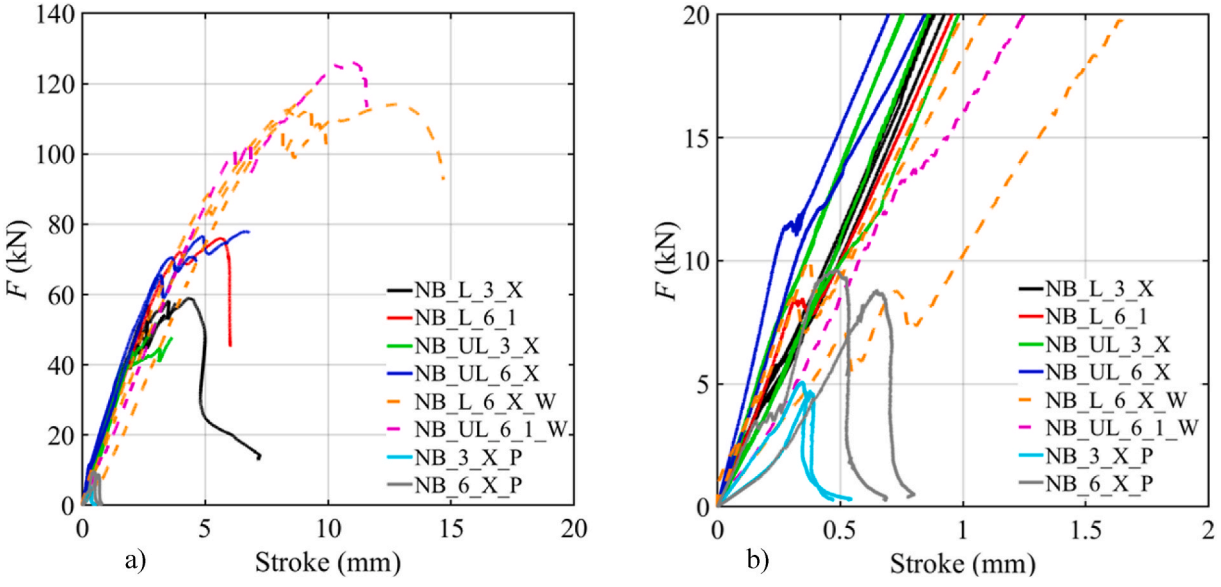

Fig. 13. Load responses for all notched beams: a) applied load (F) versus machine stroke; and b) a call-out of the first part of the responses shown in Fig. 13a.

softening behavior that could be caused by the specific shear crack pattern. The remaining GFRP-RC notched beams without CFRP wrap failed abruptly at different loading points and their load responses is pseudo-linear up to failure. The GFRP-RC notched beams with CFRP wrap feature a final nonlinear behavior at the end of the second pseudo-linear response, followed by a brief softening response. For those specimens, the test was stopped due to safety concerns, as the support steel cylinders were nearly at the edge of the steel plates attached to the bottom of the beams. The call-out Fig. 13b shows that due to the compliance of the test set-up and machine, the initial responses are not consistent among different responses. However, the features of the load responses for different groups of specimens are consistent among each group of specimens.

4.2. Applied load versus CMOD

The applied load (F) versus the CMOD responses are shown in Fig. 14a, and a call-out of the initial part of the responses are shown in Fig. 14b. The CMOD response was not recorded for the CFRP-wrapped GFRP-RC notched beams due to safety concerns for the clip-on gauge. The responses in Fig. 14a are consistent across different groups of specimens. Fig. 14b shows that the initial responses of NB_3_X_P and NB_6_X_P specimens is linear. The linear part is followed by a brief non-linear response prior to reaching the first peak load (F_{max}).

The post-peak descending part features a long tail before the test was stopped when the load was between 3 % and 5 % of F_{max}. All NB_3_X_P and NB_6_X_P specimens show consistent responses for the same width of the beam. This consistency in the load responses indicates that the concrete had almost constant properties. The GFRP-RC notched beams show the same features discussed earlier for the applied load versus stroke responses. Fig. 14b shows that the transition portion of the F-CMOD responses after reaching F_{max}, is slightly different between GFRP-RC notched beams with UL and L bars. For the former, the change in the derivative of the F-CMOD response with respect to CMOD is smoother and the change in the derivative values is within a smaller range. Ultimately, the F-CMOD responses tend to have the same slope, regardless of the bar surface condition (L or UL). It could be assumed that the absence of lacquer coating on the UL bars resulted in a slightly different local bond mechanism when the concrete crack propagation initiated. However, the pull-out test results discussed earlier (Fig. 6) did not show any influence of the lacquer coating in terms of peak load. The bond mechanism in flexure might be different compared to that of pull-out tests. Additional comments will be provided in the following.

4.3. Free end slip in GFRP-RC notched beams

Two LVDTs were used to measure the free end slip in GFRP-RC notched beams without CFRP wrap. Measurements from the left and right LVDTs (Fig. 4c) were labeled as Δ_L and Δ_R, respectively. The sum of these two measurements was labeled as $\Delta_{total} = \Delta_L + \Delta_R$. Fig. 15a shows the relationship between applied load (F) and $\Delta_{total}/2$ for all GFRP-RC notched beams with L bars, together with the F-CMOD responses. Half of the Δ_{total} represents the average free end movement of the bar with respect to concrete. Fig. 15a shows that the free end slip for these specimens is negligible compared to the CMOD. However, a recent study by the authors [43] found significant free end slip (up to approximately 2 mm) in notched beams with the same geometrical characteristic as those presented in this study but reinforced with sand-coated GFRP bars helically wrapped by a carbon fiber bundle. To better understand the free end slip in

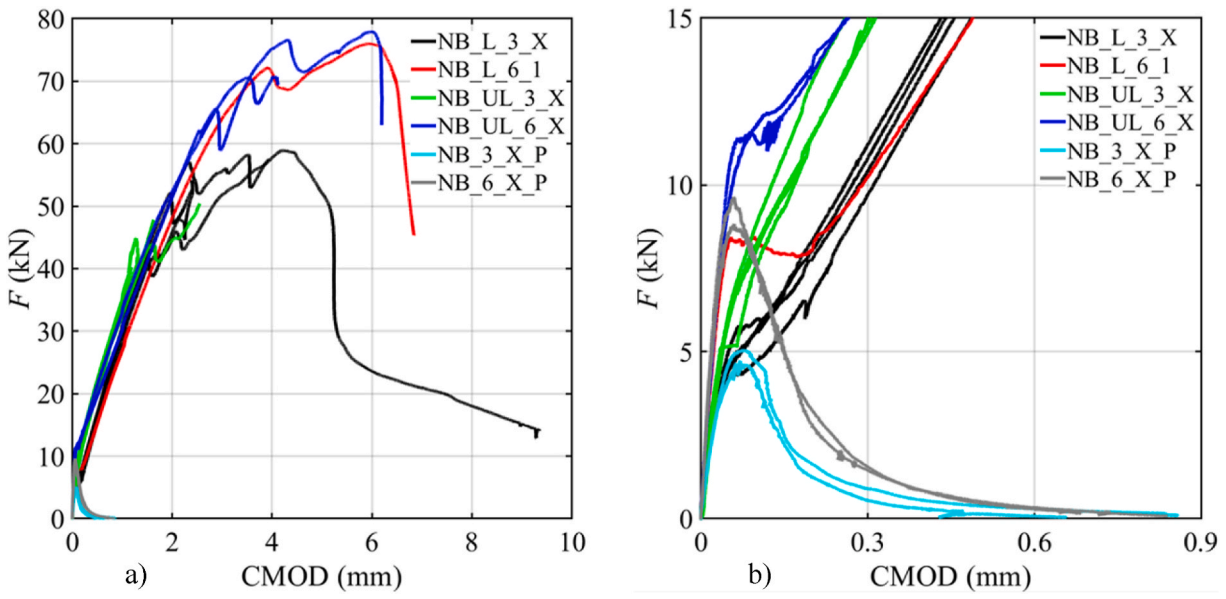

Fig. 14. Load responses for all notched beams equipped with clip-on gauge: a) applied load (F) versus CMOD; and b) a call-out of the first part of the responses shown in Fig. 14a.

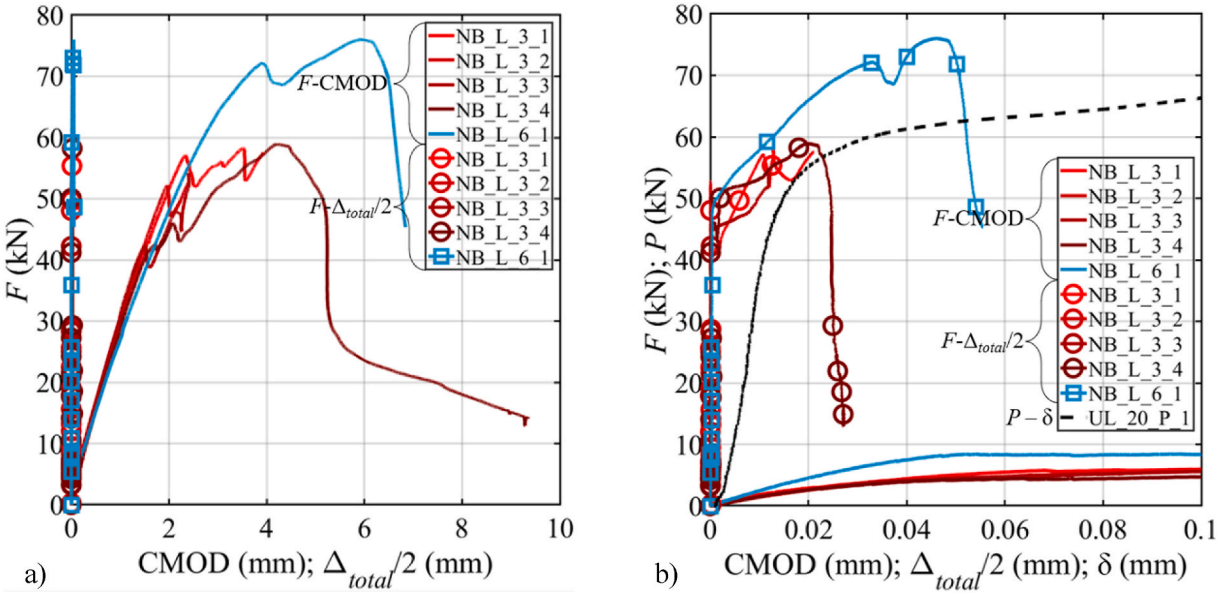

Fig. 15. Applied load versus the free end slip and CMOD: a) for notched beams with L bars; and b) call-out of the first part of the response of Fig. 15a.

these specimens, the initial part of the responses in Fig. 15a is shown in Fig. 15b. The maximum value of $\Delta_{total}/2$ for these specimens is 0.055 mm (NB_L_6_1), which is nearly negligible compared to both CMOD and the observed 2 mm free end slip in the previous study [43]. Additionally, it can be observed that free end slip begins after 40 kN of applied load, a higher value than in the previous study [43], where free end slip started at an applied load lower than 5 kN. Similar trends were observed in GFRP-RC notched beams with UL bars, though these results are not presented for the sake of brevity. The significant difference in free end slip in notched beams reinforced with sand-coated bars and those used in this study indicates that the stress transfer mechanism might develop over a different bonded length for those two types of bars. This observation is also confirmed by the different bonded length needed to reach rupture of the fibers in pull-out tests with those two types of bars, as mentioned above. The current specimens failed in shear prior to reaching maximum loading capacity (except for those that were wrapped with CFRP). The load attained by the notched beams reinforced with sand-coated bars was similar to that of specimens herein presented and without the CFRP wrap. In those beams, shear failure did not occur, but the specimens did not reach a value of the applied load that would have corresponded to the rupture of the fibers. This difference between the two bar types further supports the observation that the bonded length used in notched beams might

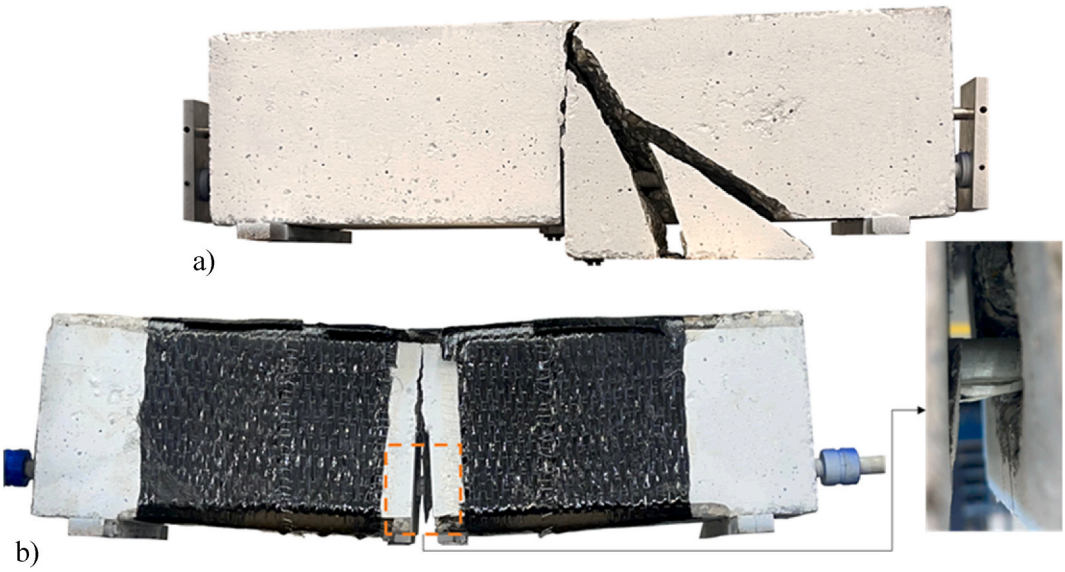

Fig. 16. a) NB_L_6_1 failed by shear cracking; b) NB_UL_6_1_W failed by the fiber rupture of the UL bar at mid-span.

have corresponded to a different development of the shear stresses along the bar-concrete interface.

For comparison, Fig. 15b also shows the *P*-δ response of Batch B concrete UL_20_P_1, which was the only specimen with bonded length equal to $20d_b$ that was equipped with LVDTs to measure δ. Although this specimen was cast using a different batch of concrete, the results presented in Section 3.3 suggest that the initial response of specimens from both batches of concrete were consistent. The comparison in terms of free end slip between pull-out and TPB test specimens is useful because the bonded length between the notch plane and one end of the beam was approximately equal to $20d_b$. The load applied in the pull-out test (*P*) can be directly compared to the load in the TPB test (*F*) because of geometrical dimensions of notched beams used in this study [43]. Fig. 15b suggests that the curves from both types of tests exhibit a similar trend and a change in slope at similar load levels.

4.4. Failure modes

For all the notched beams, microcracking started in the region surrounding the notch tip prior to reaching the first peak load (F_{max}) or any noticeable change in slope was observed. In the case of unreinforced notched beams, crack propagation corresponded to the descending portion of the load response. The test was stopped for unreinforced notched beams when crack propagation reached the top outermost fibers of the beam at a load between 3 % and 5 % of F_{max}. Similarly, in GFRP-RC notched beams without CFRP wrap, the crack propagated toward the top outermost fibers after the change of slope in the load response. These specimens failed due to shear cracking (Fig. 16a). For GFRP-RC notched beams with CFRP wrap, a nonlinear response was observed toward the end of the test, which indicated that the GFRP bar was experiencing large slips with respect to concrete and the bar was reaching the rupture of fibers. Eventually, all notched beams with CFRP wrap failed due to rupture of the bar fibers (Fig. 16b). The CFRP wrap appeared effective in preventing shear cracking.

4.5. Force versus load point displacement from DIC

DIC was used to obtain the full field displacement and strain components for one of the side faces of the notched beams. This analysis was only performed on GFRP-RC notched beams without CFRP wrap, except for beam NB_L_3_3, which was excluded due to technical issues with the DIC software during testing. The details of the DIC data correlation and the procedure to obtain the load point displacement (Δ) from the DIC displacement field are discussed in Refs. [43,52]. In brief, virtual sensors were used to measure the displacement of the load point and the supports. The latter was subtracted from the former. The virtual sensor was a square within which the vertical displacements were averaged. Fig. 17a shows the *F*-Δ responses obtained from the DIC data. The consistency of these curves among different specimens can be seen from Fig. 17a. Although the *F*-stroke responses shown in Fig. 13 were not consistent among different specimens due to the compliance of the test set-up and machine, the *F*-Δ responses obtained from DIC are consistent in terms of initial stiffness. Fig. 17b, a call-out of the first part of Fig. 17a responses, further shows this consistency across different specimen groups.

4.6. Fracture process zone from contour plots

The contour plots in Figs. 18 and 19 show the horizontal strain component (ε_{xx}) for specimens NB_L_3_1 and NB_UL_3_2, respectively (reference system shown in Fig. 4). These contour plots are capped at a strain (ε_t) corresponding to the tensile strength of the concrete. ε_t is computed as:

$$\varepsilon_t = \frac{\vec{f}_t}{E_c} \tag{3}$$

where $\vec{f}_t$ is 3.86 MPa (average splitting tensile strength performed at 67 days from the day of casting) and concrete elastic modulus (E_c) is 40.8 GPa (obtained using the *F*-CMOD responses of unreinforced notched beams [43,49]).

Each specimen is represented by three contour plots corresponding to different load values (Point A, Point B, and Point C), as indicated by colored circles in Figs. 18 and 19. The contour plots show no stress concentration on the surface of the specimens at the GFRP bar level. The contour plots capped at ε_t allow to identify the fracture process zone (FPZ) bulb [43,53]. The FPZ is the region where softening behavior of concrete in tension occurs [53]. The size of the FPZ bulb remains consistent regardless of the bar type (L or UL).

4.7. Force in the GFRP bar from cross-sectional analysis and DIC

The force in the GFRP bar (P_{bar}) in notched beams was obtained by performing cross-sectional analysis at the mid-span of the notched beam. The details of the cross-sectional analysis can be found in Refs. [43,52]. The softening behavior of concrete in tension was defined by Petersson's bilinear softening curve [54], which expresses the relationship between the stress transferred between the faces of the crack and the opening of the crack itself. The fracture energy (G_F) of the unreinforced notched beams was determined using the work-of-fracture method [55–57] and its average was calculated as 195 N/m. Parameters characterizing the softening region – such as the starting point (i.e., beginning of the FPZ), length, and the location of the neutral axis (N.A.) – were identified, for each load point, through DIC analysis using ε_{xx} profiles, as detailed in Refs. [43,52]. The crack opening corresponding to the softening behavior of concrete in the spirit of the cohesive crack model [58] was obtained using the Δu_x profile [43,52]. Two squares were selected on the

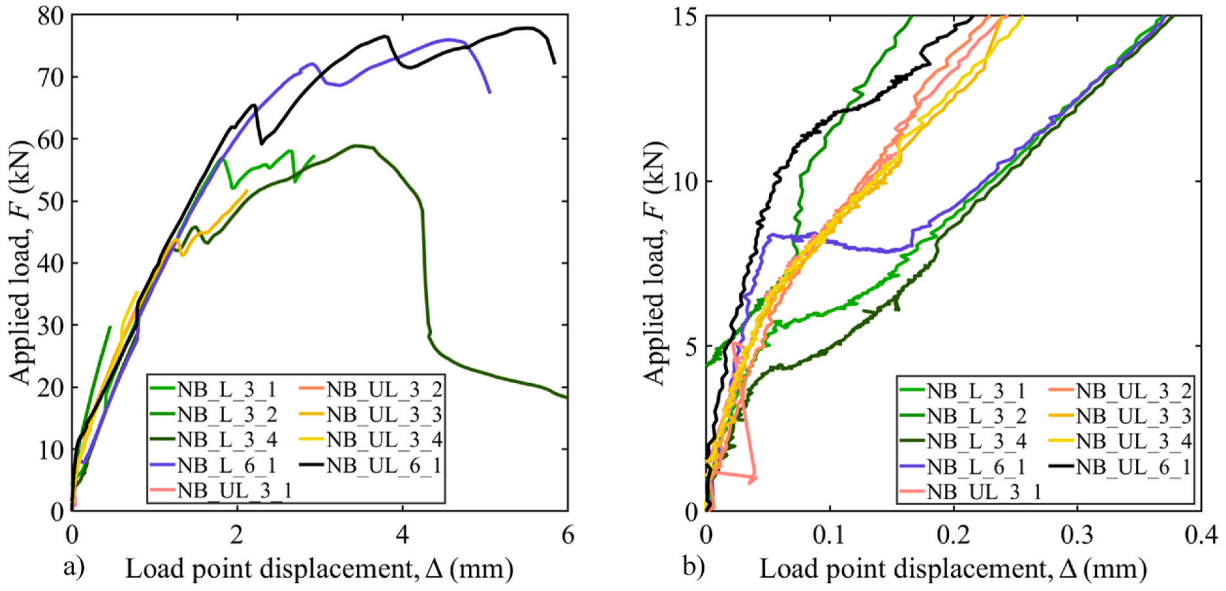

Fig. 17. Load responses obtained from the DIC analysis: a) applied load versus the load point displacement; and b) a call-out of the first part of the response in Fig. 17a.

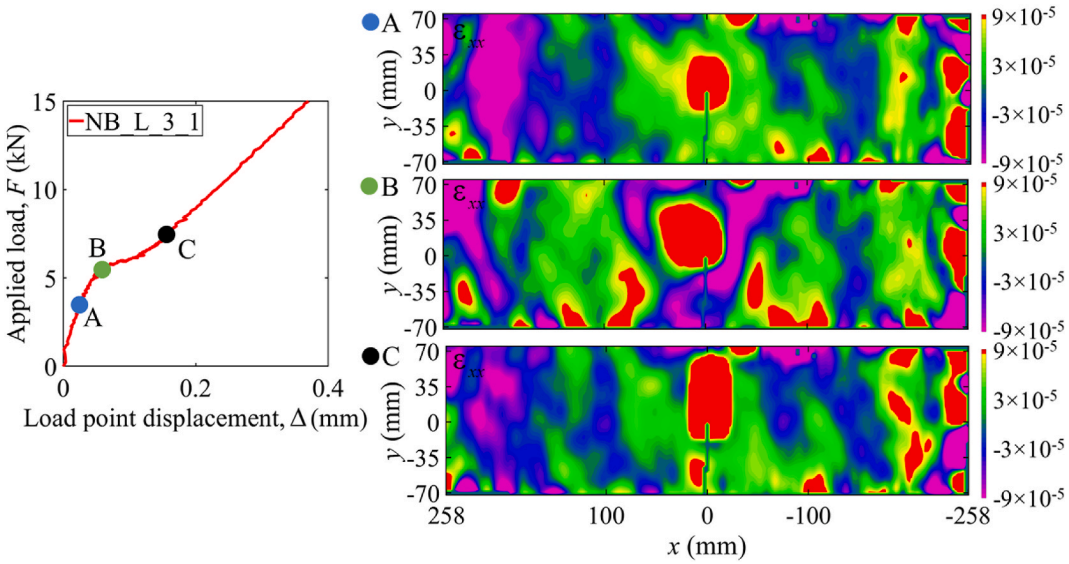

Fig. 18. Contour plots of ε_{xx} considering three different load values for NB_L_3_1.

opposite sides of the notch ligament to compute the averages of the horizontal displacements u_x, which were then subtracted to obtain Δu_x. P_{bar} was computed by applying moment equilibrium. Additionally, the slip g of the GFRP bar with respect to the surface of the notch was determined through DIC analysis, using a similar procedure as that adopted for Δu_x. Two squares were taken, each with sides of 10 mm, positioned on either side of the notch with centroids aligned with the axis of the GFRP bar (see sketch within the plot of Fig. 20a). The distance between the centers of these squares was denoted as ψ. The average horizontal displacements within these squares were calculated and then subtracted from each other to determine Δu_ψ. Finally, g was computed by subtracting the elastic deformation of the GFRP bar.

$$g = \frac{\Delta u_\psi - \frac{P_{bar}\psi}{A_b E_b}}{2} \tag{4}$$

Dividing Eq. (4) by 2 is based on the assumption that equal slip occurred on both sides of the notch. In Fig. 20, the resulting P_{bar} values were plotted against g. The use of the symbol g was chosen to recall the loaded end slip in pull-out tests. In fact, Fig. 20a includes

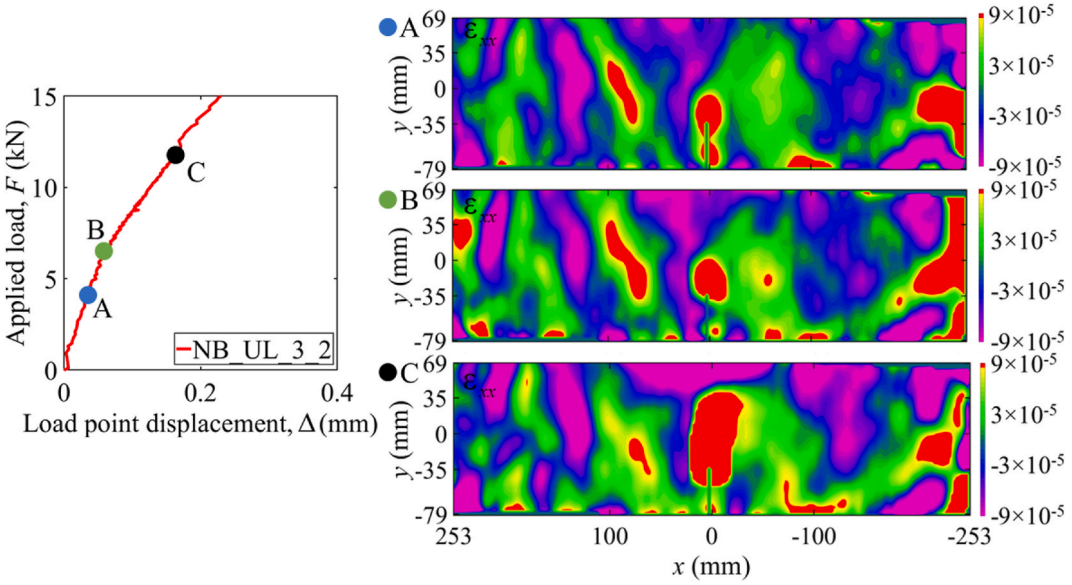

Fig. 19. Contour plots of ε_{xx} considering three different load values for NB_UL_3_2.

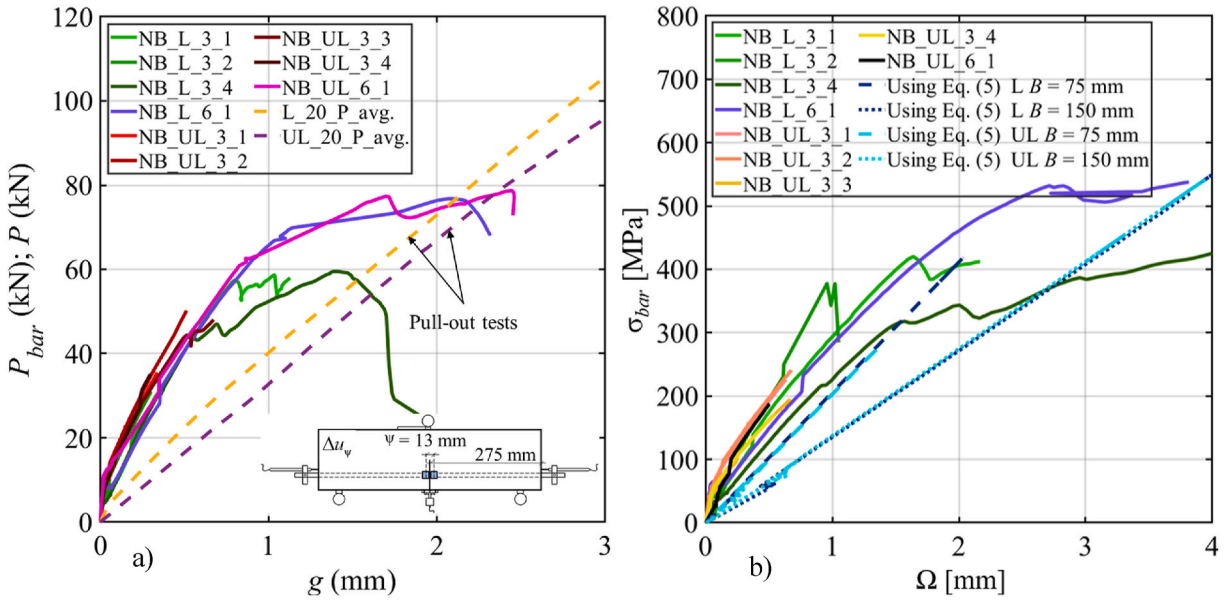

Fig. 20. a) Force in the GFRP bar versus the slip in NB_L_3_X, NB_L_6_1, NB_UL_3_X, and NB_UL_6_X specimens (using cross-section analysis) and in pull-out tests of $20d_b$ bonded length using both L and UL bars; and b) stress in the GFRP bar versus the crack opening obtained from DIC analysis and using Eq. (5) [59].

the average *P-g* responses for Batch A-concrete $\ell = 20d_b$ pull-out test specimens (with protruding ends) using L and UL bars to compare them with the P_{bar}-*g* responses. The $\ell = 20d_b$ pull-out specimens were chosen as the most representative specimens considering the bonded length in one half of the GFRP-RC notched beams. The specimens with protruding ends were selected to create similar conditions to that of the notched beams. The comparison of the P_{bar}-*g* and *P-g* responses suggests that pull-out tests can be considered a lower bound for the behavior of the bar in TPB tests. In a previous study by the authors [43], using a sand-coated GFRP bar, it was found that pull-out tests were considered an upper bound. Although the nominal diameter was the same and tensile strength of the GFRP bars used in both studies were similar, the differences in bar surface (helical lugs versus sand coating) appears to impact their bond behavior, as discussed above. This observation requires some additional comments. The effect of transversal stresses (i.e., perpendicular to the bar) are typically neglected in the cross-sectional analysis of beams. If the transversal stresses are considered and are compression stresses, they would affect bond. This effect depends on the stress transfer mechanism between the bar and concrete. If

a bar (like the one in this study) has a relatively short stress transfer zone or effective bond length, then the effect of transversal compression stresses is more pronounced. If the bar (like the one in the previous study [43]) has a long effective bond length, then the effect of the transversal stresses is less impactful. Thus, transversal stresses have a higher effect on the ribbed bars herein studied with respect to the sand-coated bars of [43], which translates into an opposite comparison between pull-out and notched beam specimens. In turn, the different behavior is related to the effective bond length, which is influenced by the surface condition. To contextualize the difference between the two types of bars, it should be recalled that to reach failure in tension of the bar in pull-out tests, a bonded length equal to $40d_b$ was needed for the sand-coated bars [43]. Conversely, the bars in this study require a bonded length of $20d_b$ to reach failure in tension in pull-out tests.

The crack opening (Ω) at the outermost bottom fibers of the beam was determined using DIC analysis. Two rectangles, each measuring 10 mm in width and 5 mm in height, were positioned at the edges of the notch. The average horizontal displacement within each rectangle was calculated and then subtracted from each other to obtain Ω. Fig. 20b shows the relationship between the tensile stress in the GFRP bar (σ_{bar}) and Ω for GFRP-RC notched beams without CFRP wrap. The stress σ_{bar} was obtained dividing P_{bar} by A_b. The results show that neither the type of bar (L or UL) nor the width of the notched beams have a significant effect on the responses. The crack opening was also calculated using the equation provided in Ref. [59]:

$$\Omega = 2\frac{\sigma_{bar}}{E_b}\beta k_b\sqrt{{d_c}^2 + \left(\frac{b_s}{2}\right)^2} \tag{5}$$

where $d_c = 44.5$ mm is the distance between the bottom part of the beam to the center of the GFRP bar location and b_s is the spacing of the GFRP bar. b_s was taken as 75 mm and 150 mm for $B = 75$ mm and $B = 150$ mm width specimens, respectively. $\beta = m/n$, where m is the distance of the bottom face of the beam to the neutral axis (N.A.) of the beam and n is the distance of the GFRP bar layer to the N.A. location. The N.A. was obtained from the DIC analysis. The bond-dependent coefficient (k_b) was taken as 1.2 as recommended in Ref. [59]. Using Eq. (5), the opening of the crack was computed considering both the width of the notched beams and also the type of the GFRP bar (L and UL have a different elastic modulus). Fig. 20b shows that the crack opening (Ω) obtained using Eq. (5) for $B = 75$ mm closely resembles the crack opening in notched beams obtained from DIC analysis, regardless of the bar coating. However, in general, the comparison of the $\sigma_{bar} - \Omega$ obtained from Eq. (5) with the responses obtained from DIC analysis shows that the former behaves as a lower bound. In a previous study by the same authors, using a sand-coated GFRP bar, the $\sigma_{bar} - \Omega$ obtained from Eq. (5) behaved as an upper bound. This observation further supports the fact that the bond behavior of the bars herein presented is different from that of the sand-coated bars.

5. Conclusion

A comprehensive GFRP bar-concrete bond behavior was investigated using the pull-out tests and TPB tests of notched beams. Two types of GFRP bars with identical geometry but varying surface conditions were used. One bar surface was finished with lacquer (named L bars), while the other had no lacquer (referred to as UL bars). Both bars featured helical lugs on their surfaces. Pull-out specimens were cast from two distinct concrete batches: one with high-strength concrete (Batch A) and the other with low-strength concrete (Batch B). The notched beams were cast only from the high-strength concrete batch. The study analyzes the load responses and draws the following conclusions.

1) The average peak loads in pull-out specimens using lacquered and unlacquered GFRP bars were higher than those of another GFRP bar with comparable geometry but featuring a sand coating, as studied by the same authors.
2) The variation in GFRP bar surface coating did not appear to affect the bond behavior between the GFRP bar and concrete when the peak loads of the pull-out tests were considered.
3) Specimens cast from higher-strength concrete, with free end bars cut and lacquered bars, showed higher peak loads in $10d_b$ bonded length specimens compared to those from lower-strength concrete. However, this behavior was not seen in $5d_b$ bonded length specimens. It can be assumed that the shorter bonded length might not sufficiently reflect the influence of concrete strength in $5d_b$ specimens. Lacquered bars with free end protruded bars from high-strength concrete showed higher loads even with a $5d_b$ bonded length, surpassing the specimens from lower concrete strength. The protruding free end bar part showed increased resistance from higher-strength concrete, resulting in higher peak loads. The impact of concrete strength on unlacquered bars was similar to that of lacquered bars.
4) Specimens featuring lacquered and unlacquered bars with free end protrusion from higher-strength concrete consistently showed an approximately 30 kN increase in peak loads, irrespective of bonded length or bar surface coating over the specimens with free end cut. Similarly, specimens from lower-strength concrete consistently demonstrated higher peak loads for those with free end protrusion over the free end cut specimens, although the increase in peak loads was not as substantial as in the higher-strength concrete specimens. It can be assumed that both free end protrusion and concrete strength influenced to generate higher peak loads simultaneously.
5) The free end slip did not show any discernible impact attributable to concrete strength, surface coating, or free end conditions.
6) Irrespective of the bar surface coating, the average bond strength of specimens with a protruded free end bar appeared to decrease as the bonded length increased. In contrast, for specimens with the free end cut, there was an increase in average bond strength from $5d_b$ to $10d_b$, followed by a decrease from $10d_b$ to $20d_b$.

7) The bond strength corresponding to peak loads in Batch A-concrete $5d_b$ bonded length specimens was approximately twice that of Batch B-concrete $5d_b$ bonded length specimens, considering both lacquered and unlacquered bars. This difference in bond strength due to concrete strength was also observed in $10d_b$ and $20d_b$ bonded length specimens, although not as pronounced as in the $5d_b$ bonded length specimens, as the different concrete strength is also related to the effect of the protrusion of the bar, which decreases as the bonded length increases.
8) The bond strength evaluated with pull-out tests depends on the bonded length and free end condition. This indicates that the bar-concrete interfacial shear stress is not constant along the bonded length and depends on the presence of the protruding part of the bar. Based on the results presented, bonded lengths greater than prescribed in guidelines ASTM D7913 and ISO 10406-1 should be adopted when pull-out test results are used to determine the bond properties to be introduced in mechanical models for the determination of bond-dependent structural parameters such as the anchorage length and crack spacing and opening in structural elements. In addition, the protruding part of the bar should be avoided since it is not present in structural elements.
9) The negligible free end slip in notched beams suggests the stress transfer mechanism might develop over a shorter bonded length for the two types of bars used in this study compared to the sand-coated GFRP bar used in a previous study [43] by the same authors.
10) The comparison of applied load versus slip from notched beams and pull-out tests suggests that the pull-out tests can be considered a lower bound for the behavior of the bar in TPB tests. In the previous study [43], the trend was opposite. The authors argue that the difference between notched beam and pull-out tests depend on the length of the stress transfer zone. As stresses normal to the bar arise in the notched beam specimens, their effect is more pronounced if the effective bond length is short since higher shear stresses are distributed within a shorter length near the mid-span, where the normal (compressive) stresses develop.

CRediT authorship contribution statement

Mohammod Minhajur Rahman: Writing – original draft, Investigation, Data curation. **Charles T. Cope:** Writing – review & editing, Investigation. **Iman Abavisani:** Writing – review & editing, Investigation. **Tommaso D'Antino:** Writing – review & editing, Validation, Methodology, Conceptualization. **Francesco Focacci:** Writing – review & editing, Validation, Methodology, Conceptualization. **Christian Carloni:** Writing – review & editing, Validation, Supervision, Resources, Methodology.

Declaration of competing interest

The authors declare that they have no known competing financial interests or personal relationships that could have appeared to influence the work reported in this paper.

Data availability

Data will be made available on request.

References

[1] Y. Miyano, M. Nakada, Accelerated testing methodology for durability of CFRP, Compos. B Eng. 191 (2020) 107977, https://doi.org/10.1016/j.compositesb.2020.107977.
[2] P. Bodzak, Prestressing and preloading effect in RC slabs strengthened with normal and pretensioned CFRP EBR strips, Compos. B Eng. 169 (2019) 19–28, https://doi.org/10.1016/j.compositesb.2019.03.079.
[3] G. Foret, O. Limam, Experimental and numerical analysis of RC two-way slabs strengthened with NSM CFRP rods, Constr. Build. Mater. 22 (2008) 2025–2030, https://doi.org/10.1016/j.conbuildmat.2007.07.027.
[4] G. Qin, J. Na, W. Mu, W. Tan, J. Yang, J. Ren, Effect of continuous high temperature exposure on the adhesive strength of epoxy adhesive, CFRP and adhesively bonded CFRP-aluminum alloy joints, Compos. B Eng. 154 (2018) 43–55, https://doi.org/10.1016/j.compositesb.2018.07.059.
[5] P. Bodzak, Flexural behaviour of concrete beams reinforced with different grade steel and strengthened by CFRP strips, Compos. B Eng. 167 (2019) 411–421, https://doi.org/10.1016/j.compositesb.2019.02.056.
[6] M. Haji, H. Naderpour, A. Kheyroddin, Experimental study on influence of proposed FRP-strengthening techniques on RC circular short columns considering different types of damage index, Compos. Struct. 209 (2019) 112–128, https://doi.org/10.1016/j.compstruct.2018.10.088.
[7] J.R. Cruz, S. Seręga, J. Sena-Cruz, E. Pereira, A. Kwiecień, B. Zając, Flexural behaviour of NSM CFRP laminate strip systems in concrete using stiff and flexible adhesives, Compos. B Eng. 195 (2020) 108042, https://doi.org/10.1016/j.compositesb.2020.108042.
[8] O. Chaallal, B. Benmokrane, Physical and mechanical performance of an innovative glass-fiber-reinforced plastic rod for concrete and grouted anchorages, Can. J. Civ. Eng. 20 (1993) 254–268, https://doi.org/10.1139/l93-031.
[9] Mark Yunovich, Neil G. Thompson, Corrosion of highway bridges: economic impact and control methodologies, Concr. Int. 25 (2003).
[10] K. Chu, K.M.A. Hossain, M. Lachemi, Fatigue behavior of GFRP-reinforced ECC link slabs under variable stress levels and number of cycles, Eng. Struct. 222 (2020) 111130, https://doi.org/10.1016/j.engstruct.2020.111130.
[11] E. Ahmed, B. Brahim, Design of bridge deck slabs using glass fiber-reinforced polymer (GFRP) bars of different grades. Proceedings of the 9th International Conference on Short and Medium Span Bridges (CSCE), 2014.
[12] K.-D. Peng, B.-T. Huang, L.-Y. Xu, R.-L. Hu, J.-G. Dai, Flexural strengthening of reinforced concrete beams using geopolymer-bonded small-diameter CFRP bars, Eng. Struct. 256 (2022) 113992, https://doi.org/10.1016/j.engstruct.2022.113992.
[13] J.-X. Zhu, K.-F. Weng, B.-T. Huang, L.-Y. Xu, J.-G. Dai, Ultra-High-Strength Engineered Cementitious Composites (UHS-ECC) panel reinforced with FRP bar/grid: development and flexural performance, Eng. Struct. 302 (2024) 117193, https://doi.org/10.1016/j.engstruct.2023.117193.
[14] J.-X. Zhu, K.-F. Weng, W.-H. Liu, B.-T. Huang, K.-D. Peng, J.-H. Zhu, et al., Thin-layer Ultra-High-Strength Engineered Cementitious Composites (UHS-ECC) reinforced with small-diameter FRP bars for structural strengthening, Thin-Walled Struct. 205 (2024) 112592, https://doi.org/10.1016/j.tws.2024.112592.

[15] V. Carvelli, M.A. Pisani, C. Poggi, High temperature effects on concrete members reinforced with GFRP rebars, Compos. B Eng. 54 (2013) 125–132, https://doi.org/10.1016/j.compositesb.2013.05.013.
[16] R. Pagani, M. Bocciarelli, V. Carvelli, M.A. Pisani, Modelling high temperature effects on bridge slabs reinforced with GFRP rebars, Eng. Struct. 81 (2014) 318–326, https://doi.org/10.1016/j.engstruct.2014.10.012.
[17] S. Spagnuolo, A. Meda, Z. Rinaldi, A. Nanni, Residual behaviour of glass FRP bars subjected to high temperatures, Compos. Struct. 203 (2018) 886–893, https://doi.org/10.1016/j.compstruct.2018.07.077.
[18] G. Portnov, C.E. Bakis, E. Lackey, V. Kulakov, FRP Reinforcing bars — designs and methods of manufacture (Review of Patents), Mech. Compos. Mater. 49 (2013) 381–400, https://doi.org/10.1007/s11029-013-9355-1.
[19] E. Nepomuceno, J. Sena-Cruz, L. Correia, T. D'Antino, Review on the bond behavior and durability of FRP bars to concrete, Constr. Build. Mater. 287 (2021) 123042, https://doi.org/10.1016/j.conbuildmat.2021.123042.
[20] A. Meda, Z. Rinaldi, S. Spagnuolo, Experimental investigation on the behaviour of concrete ties reinforced with GFRP bars, Compos. Struct. 254 (2020) 112805, https://doi.org/10.1016/j.compstruct.2020.112805.
[21] W. Chen, F. Meng, H. Sun, Z. Guo, Bond behaviors of BFRP bar-to-concrete interface under dynamic loading, Constr. Build. Mater. 305 (2021) 124812, https://doi.org/10.1016/j.conbuildmat.2021.124812.
[22] S.P. Tastani, S.J. Pantazopoulou, Bond of GFRP bars in concrete: experimental study and analytical interpretation, J. Compos. Construct. 10 (2006) 11, https://doi.org/10.1061/(ASCE)1090-0268(2006)10:5(381).
[23] S. Solyom, G.L. Balázs, Bond of FRP bars with different surface characteristics, Constr. Build. Mater. 264 (2020) 119839, https://doi.org/10.1016/j.conbuildmat.2020.119839.
[24] S. Solyom, G.L. Balázs, Analytical and statistical study of the bond of FRP bars with different surface characteristics, Compos. Struct. 270 (2021) 113953, https://doi.org/10.1016/j.compstruct.2021.113953.
[25] E. Cosenza, G. Manfredi, R. Realfonzo, Behavior and modeling of bond of FRP rebars to concrete, J. Compos. Construct. 1 (1997) 40–51, https://doi.org/10.1061/(ASCE)1090-0268(1997)1:2(40).
[26] M. Baena, L. Torres, A. Turon, C. Barris, Experimental study of bond behaviour between concrete and FRP bars using a pull-out test, Compos. B Eng. 40 (2009) 784–797, https://doi.org/10.1016/j.compositesb.2009.07.003.
[27] A. Veljkovic, V. Carvelli, M.M. Haffke, M. Pahn, Concrete cover effect on the bond of GFRP bar and concrete under static loading, Compos. B Eng. 124 (2017) 40–53, https://doi.org/10.1016/j.compositesb.2017.05.054.
[28] X. Zhao, M. Minhajur Rahman, T. D'Antino, F. Focacci, C. Carloni, Effect of bonded length on the load response and failure mode of pull-out tests of GFRP bars embedded in concrete, Constr. Build. Mater. 347 (2022) 128425, https://doi.org/10.1016/j.conbuildmat.2022.128425.
[29] N. Saleh, A. Ashour, D. Lam, T. Sheehan, Experimental investigation of bond behaviour of two common GFRP bar types in high – strength concrete, Constr. Build. Mater. 201 (2019) 610–622, https://doi.org/10.1016/j.conbuildmat.2018.12.175.
[30] M.R. Ehsani, H. Saadatmanesh, S. Tao, Bond behavior of deformed GFRP rebars, J. Compos. Mater. 31 (1997) 1413–1430, https://doi.org/10.1177/002199839703101404.
[31] J.-Y. Lee, T.-Y. Kim, T.-J. Kim, C.-K. Yi, J.-S. Park, Y.-C. You, et al., Interfacial bond strength of glass fiber reinforced polymer bars in high-strength concrete, Compos. B Eng. 39 (2008) 258–270, https://doi.org/10.1016/j.compositesb.2007.03.008.
[32] ASTM D30. ASTM D7913/D7913M-14, Standard Test Method for Bond Strength of Fiber-Reinforced Polymer Matrix Composite Bars to Concrete by Pullout Testing, 2020.
[33] ISO, Fibre-reinforced Polymer (FRP) Reinforcement of Concrete – Test Methods, ISO, 2015. https://www.iso.org/cms/render/live/en/sites/isoorg/contents/data/standard/06/36/63657.html. (Accessed 25 March 2022).
[34] X. Zhao, M.M. Rahman, T. D'Antino, F. Focacci, C. Carloni, Effect of the bar diameter on the load response of GFRP-concrete pull-out tests. https://doi.org/10.5281/ZENODO.8164966, 2023.
[35] C.T. Cope, M.M. Rahman, T. D'Antino, F. Focacci, C. Carloni, Pull-out test of FRP bars: the effect of the free end protruding portion of the bar. https://doi.org/10.5281/ZENODO.8109654, 2023.
[36] Y. Luo, P. Liao, R. Pan, J. Zou, X. Zhou, Effect of bar diameter on bond performance of helically ribbed GFRP bar to UHPC, J. Build. Eng. 91 (2024) 109577, https://doi.org/10.1016/j.jobe.2024.109577.
[37] B. Basaran, I. Kalkan, Investigation on variables affecting bond strength between FRP reinforcing bar and concrete by modified hinged beam tests, Compos. Struct. 242 (2020) 112185, https://doi.org/10.1016/j.compstruct.2020.112185.
[38] Focacci F, Cope CT, Rahman MM, D'Antino T, Carloni C. CALIBRATION OF THE GFRP-CONCRETE COHESIVE MATERIAL LAW USING PULL-OUT TESTS 2023. https://doi.org/10.5281/ZENODO.8109666.
[39] I.C. Rosa, J.P. Firmo, J.R. Correia, P. Mazzuca, Influence of elevated temperatures on the bond behaviour of ribbed GFRP bars in concrete, Cement Concr. Compos. 122 (2021) 104119, https://doi.org/10.1016/j.cemconcomp.2021.104119.
[40] K.-D. Peng, J.-J. Zeng, B.-T. Huang, J.-Q. Huang, Y. Zhuge, J.-G. Dai, Bond performance of FRP bars in plain and fiber-reinforced geopolymer under pull-out loading, J. Build. Eng. 57 (2022) 104893, https://doi.org/10.1016/j.jobe.2022.104893.
[41] Z. Achillides, K. Pilakoutas, Bond behavior of fiber reinforced polymer bars under direct pullout conditions, J. Compos. Construct. 8 (2004) 173–181, https://doi.org/10.1061/(ASCE)1090-0268(2004)8:2(173).
[42] N. Galati, B. Vollintine, A. Nanni, L.R. Dharani, M.A. Aiello, Thermal effects on bond between FRP rebars and concrete. Advanced Polymer Composites for Structural Applications in Construction, Elsevier, 2004, pp. 501–508, https://doi.org/10.1533/9781845690649.5.501.
[43] M.M. Rahman, X. Zhao, T. D'Antino, F. Focacci, C. Carloni, Digital image correlation and cracked hinge model applied to notched beams reinforced with GFRP bars, Eng. Fract. Mech. 301 (2024) 109965, https://doi.org/10.1016/j.engfracmech.2024.109965.
[44] Mateenbar USA, Inc, MATEENBAR TM certificate of analysis. Private Communication with the Manufacturer, 2021.
[45] CSA, Design and construction of building structures with fibre-reinforced polymers, CAN/CSA S806-12 (2021).
[46] ASTM C09, ASTM C39/C39M-21 - Standard Test Method for Compressive Strength of Cylindrical Concrete Specimens, ASTM International, 2020, https://doi.org/10.1520/C0039_C0039M-20.
[47] ASTM C09, ASTM C496/C496M-17 - Standard Test Method for Splitting Tensile Strength of Cylindrical Concrete Specimens, ASTM International, 2017, https://doi.org/10.1520/C0496_C0496M-17.
[48] C. Charles Tucker, M.M. Rahman, F. Focacci, T. D'Antino, I. Abavisani, C. Carloni, Quasi-Static and Fatigue Behavior of GFRP Bars Embedded in Concrete: A Comparison between Pull-Out Tests and Flexural Tests of Slabs, 360, ACI Symposium Publication, 2024, pp. 709–728, https://doi.org/10.14359/51740658.
[49] Z. Ameli, M.M. Rahman, C. Carloni, Largest experimental investigation on size effect of concrete notched beams, J. Eng. Mech. 150 (2024) 04023114, https://doi.org/10.1061/JENMDT.EMENG-7225.
[50] ASTM, ASTM C293/C293M -Standard Test Method for Flexural Strength of Concrete (Using Simple Beam with Center-Point Loading), 2016.
[51] R.J. Gravina, J. Li, S.T. Smith, P. Visintin, Environmental durability of FRP bar-to-concrete bond: critical review, J. Compos. Construct. 24 (2020) 03120001, https://doi.org/10.1061/(ASCE)CC.1943-5614.0001016.
[52] M.M. Rahman, X. Zhao, T. D'Antino, F. Focacci, C. Carloni, Fracture behavior and digital image analysis of GFRP reinforced concrete notched beams, Materials 15 (2022) 5981, https://doi.org/10.3390/ma15175981.
[53] Z.P. Bazant, J. Planas, Fracture and Size Effect in Concrete and Other Quasibrittle Materials, Routledge, 2019.
[54] P.E. Petersson, Crack growth and development of fracture zones in plain concrete and similar materials. Division of Building Materials, Lund Institute of Technology, Lund, Sweden n.d.; Report no. TVBM-1006.
[55] M. Elices, G.V. Guinea, J. Planas, Measurement of the fracture energy using three-point bend tests: Part 3—influence of cutting theP-δ tail, Mater. Struct. 25 (1992) 327–334, https://doi.org/10.1007/BF02472591.

[56] A. Hillerborg, The theoretical basis of a method to determine the fracture energyG F of concrete, Mater. Struct. 18 (1985) 291–296, https://doi.org/10.1007/BF02472919.
[57] C.G. Hoover, Z. P. Bažant, Comprehensive concrete fracture tests: size effects of Types 1 & 2, crack length effect and postpeak, Eng. Fract. Mech. 110 (2013) 281–289, https://doi.org/10.1016/j.engfracmech.2013.08.008.
[58] A. Hillerborg, M. Modéer, P.-E. Petersson, Analysis of crack formation and crack growth in concrete by means of fracture mechanics and finite elements, Cement Concr. Res. 6 (1976) 773–781, https://doi.org/10.1016/0008-8846(76)90007-7.
[59] C. Shield, V. Brown, C.E. Bakis, S. Gross, A recalibration of the crack width bond-dependent coefficient for GFRP-reinforced concrete, J. Compos. Construct. 23 (2019) 04019020, https://doi.org/10.1061/(ASCE)CC.1943-5614.0000978.